Applications in Energy and Combustion Science 21 (2025) 100320

Contents lists available at ScienceDirect

Applications in Energy and Combustion Science

journal homepage: www.sciencedirect.com/journal/applications-in-energy-and-combustion-science

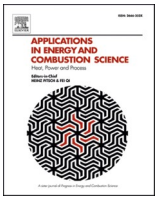

Comprehensive reevaluation of acetaldehyde chemistry - part I: Assessment of important kinetic parameters and the underlying uncertainties

Xinrui Ren [a], Hongqing Wu [a], Ruoyue Tang [a], Yanqing Cui [a], Mingrui Wang [a], Song Cheng [a,b,*]

[a] Department of Mechanical Engineering, The Hong Kong Polytechnic University, Kowloon 999077, Hong Kong
[b] Research Institute for Smart Energy, The Hong Kong Polytechnic University, Kowloon 999077, Hong Kong

ARTICLE INFO

Keywords:
Acetaldehyde chemistry
Physics-based model reevaluation
Model validation and comparison
Uncertainty analysis

ABSTRACT

Understanding the combustion chemistry of acetaldehyde is crucial to developing robust and accurate combustion chemistry models for practical fuels, especially for biofuels. This study aims to re-evaluate the important rate and thermodynamic parameters for acetaldehyde combustion chemistry and determine the physical uncertainties of these parameters. The rate parameters of 79 key reactions are reevaluated using > 100,000 direct experiments and quantum chemistry computations from > 900 studies, and the thermochemistry (Δh_f(298 K), s^0(298 K) and c_p) of 24 key species are reevaluated based on the ATCT database, the NIST Chemistry WebBook, the TMTD database, and 35 published chemistry models. The updated parameters are incorporated into a recent acetaldehyde chemistry model, which is further assessed against available fundamental experiments measurements (10 RCM-IDT, 123 ST-IDT, 633 JSR-species concentrations, and 102 flow reactor-species concentrations) and existing chemistry models, with clearly better performance obtained in the high-temperature regime. Sensitivity and flux analyses further highlight the insufficiencies of previous models in representing the key pathways, particularly the branching ratios of acetaldehyde- and formaldehyde-consuming pathways. Meanwhile, temperature-dependent and temperature-independent uncertainties are statistically evaluated for kinetic and thermochemical parameters, respectively, where the large differences between the updated and the original model parameters reveal the necessity of reassessment of kinetic and thermochemical parameters completely based on direct experiments and theoretical calculations for rate and thermodynamic parameters. The application of the determined uncertainty domains of the key kinetic and thermodynamic parameters is further demonstrated through a case study, with the modelling uncertainty and its reliability highlighted. With the configured uncertainty domain of the updated acetaldehyde chemistry model, further uncertainty quantification and optimization can be conducted to improve the model performance, which is currently under progress in the authors' group.

1. Introduction

Acetaldehyde is an important intermediate and a pollutant species during the combustion of fossil fuels and biofuels. In addition, acetaldehyde chemistry marks the final steps of combustion chemistry of C_2 and heavier hydrocarbons [1] (particularly alcohols [2,3]), and combustion chemistry models for these hydrocarbons have been constructed based on the acetaldehyde chemistry models. Therefore, understanding the combustion chemistry of acetaldehyde is crucial to developing robust and accurate combustion chemistry models for practical fuels, especially for biofuels.

Acetaldehyde chemistry has been extensively studied in the past. The earliest article on acetaldehyde combustion can be dated back to 1934, where Rice and Herzfeld [4] first proposed and analyzed a reaction set for acetaldehyde decomposition. Following this, Beeley et al. [5] devised a high-temperature reaction mechanism for acetaldehyde and compared the modeling results with ignition delays obtained in a shock tube (ST) at equivalence ratios 0.5–3.0 and temperatures from 1550 to 1850 K. Later, Kaiser et al. [6] carried out acetaldehyde oxidation experiments using a low-pressure static reactor over the low-temperature range of 553 - 713 K. A reaction mechanism of acetaldehyde was constructed which was able to fairly predict experimental features and quantitative product concentrations. Borisov et al. [7] developed another reaction mechanism of acetaldehyde oxidation at intermediate and high

* Corresponding authors at: Department of Mechanical Engineering, The Hong Kong Polytechnic University, Kowloon 999077, Hong Kong.
E-mail address: songcheng@polyu.edu.hk (S. Cheng).

https://doi.org/10.1016/j.jaecs.2025.100320
Received 5 August 2024; Received in revised form 8 December 2024; Accepted 7 January 2025
Available online 11 January 2025

temperatures, which was subsequently validated through a series of experiments.

Apart from the early studies as mentioned above, more experimental efforts have been addressed to understand acetaldehyde combustion chemistry since 2000. Dagaut et al. [8] studied the oxidation of acetaldehyde in a jet-stirred reactor (JSR) at temperatures of 900 - 1300 K and pressures of 1 - 10 atm. Ignition delay times in a shock tube were also measured under a wide range of conditions ($0.5 \leq \Phi \leq 2$, 1230 - 2530 K, 2 - 5 atm). Won et al. [9] measured the ignition delay of acetaldehyde behind a reflected shock wave at high temperatures, i.e., 1320 - 1897 K, at 100 torr, and a mechanism consisting of 34 species and 110 reactions was proposed. Yasunaga et al. [10] reported a shock tube and modeling study of acetaldehyde pyrolysis and oxidation (1000 - 1700 K, 1.2 - 2.8 bar). They developed a detailed mechanism containing 50 species and 178 reactions. Mével et al. [11] also studied high-temperature pyrolysis and oxidation of acetaldehyde in a shock tube at 1295 - 1580 K and 306 - 404 kPa. They excluded reactions related to low-temperature oxidation and simulated the measured ignition delay times of acetaldehyde with reasonable agreement achieved. Tao et al. [12] measured the chemical structures of low-pressure laminar premixed acetaldehyde flames at equivalence ratios of 1.7 and 1.0. They identified and quantified about 40 species in the post-flame zone, which provided more detailed information on the high-temperature chemistry of acetaldehyde combustion. Recently, Zhang et al. [13] focused on the chain-branching reactions which affected the low-temperature oxidation rate of acetaldehyde and developed a kinetic model of acetaldehyde. Low-temperature JSR oxidation of acetaldehyde was also carried out at a range of thermodynamic and fuel loading conditions ($0.5 \leq \Phi \leq 4$, 460 - 900 K, 710 - 720 Torr), and a variety of reactive species were identified and quantified. They found that newly added reactions, such as H-atom abstraction from acetaldehyde by methyl peroxyl radical, had great impact on modeling results. Additionally, Tao et al. [14] also developed a new kinetic model for the oxidation of acetaldehyde recently, based on their previous study [15]. They reported the mole fraction profile of 31 species in a counterflow flame at 600 Torr and ignition delay times at 10 atm and 700 - 1100 K in a rapid compression machine (RCM), and validated the new kinetic model using these experiments. Hashemi et al. [16] developed a detailed chemical kinetic model for the oxidation of acetaldehyde at intermediate to high temperature and elevated pressure. They conducted flow reactor experiments at 600 - 900 K and pressures of 25 and 100 bar. Wako et al. [17] also developed a detailed acetaldehyde mechanism through an automated algorithm, which was validated against the measured ignition delay times ($\Phi \leq 2$, 1250 – 1700 K, 1.6 - 4 atm) and laminar burning velocity ($0.6 \leq \Phi \leq 1.6$, 1 atm).

Despite the studies as reviewed above, the relevant experimental studies on acetaldehyde fundamental combustion behaviors are still lacking, particularly those at high pressure conditions that are more relevant to advanced propulsion systems. In fact, acetaldehyde chemistry has been somewhat overlooked and ill-conditioned in existing models for large hydrocarbons, as critically pointed out by Cheng et al. [18] in a recent study, where an ethanol chemistry model and a gasoline surrogate chemistry model agreed well with the high-pressure ignition delay times of ethanol and gasoline surrogates, respectively, while showing great errors for acetaldehyde.

On the other hand, chemistry models can be improved in a systematic manner with a reasonable amount of effort using uncertainty quantification (UQ) and optimization frameworks. Different approaches have been developed for UQ and optimization of chemical kinetic models. The underlying frameworks can be categorized as either probabilistic or deterministic, depending on how the uncertainty is treated. The most influential deterministic approach is the "bound-to-bound data collaboration" (B2B-DC) pioneered by Frenklach and co-workers [19], which prescribes fixed uncertainty bounds for involved parameters and determines the overall model uncertainty using the maximum and minimum of the simulation results. In contrast, probabilistic approaches address the uncertainty of the parameters and the model with probability density functions, such as the polynomial chaos expansion (MUM-PCE) method developed by Wang and co-workers [20], the global parameter optimization algorithm (GPOA) developed by Turányi and co-workers [21], and the ANN-MCMC method developed by Yang and co-workers [22]. Both the deterministic and probabilistic approaches can be used to optimize chemical kinetic models, known as the *reverse* problems. For instance, the use of B2B-DC to optimize a recent syngas model [23], MUM-PCE to optimize the USC Mech II [24], and GPOA to optimize a methanol model [25,26]. These methods have been proved very effective to improve the accuracy of chemistry models, which unfortunately have not been applied to acetaldehyde yet, though there is a large number of experimental and theoretical data (e.g., NIST Chemical Kinetics Database) available for the rate coefficients of elementary reactions involved in acetaldehyde chemistry.

Therefore, the objectives of this study are two-fold: (a) to reevaluate the acetaldehyde chemistry purely based the available rate and thermodynamic data; and (b) to define a chemistry model and condition its uncertainty purely based on direct physical information. To this end, all the important kinetic and thermodynamic parameters are identified and reevaluated based on $>$ 100,000 direct experiments and quantum chemistry computations from $>$ 900 studies. Following this, the reevaluated kinetic and thermodynamic parameters are incorporated into an updated model, which is further validated against all available experiments and compared among various models, and analyzed via sensitivity and flux analyses. Finally, the uncertainties of the reevaluated parameters are physically characterized, which is followed by statistical analyses of model uncertainty.

2. Experimental and computational methods

2.1. Chemical kinetic model of acetaldehyde

The last version of the acetaldehyde chemistry model developed by Tao et al. [14] is adopted in this study for further analysis, while the other models, including those proposed by Wako et al. [17], Hashemi et al. [16], Mével et al. [11], and Zhang et al. [13], are used for comparisons (as discussed in the following sections). The mechanism from [14] has been validated against a number of experimental and literature data, demonstrating reasonably good performance under wide ranges of temperatures (300 – 2300 K) and pressures (0.02 – 10 atm) [14]. It should be noted that using a different acetaldehyde model will have negligible influences as the present work will reevaluate all the important reactions in acetaldehyde chemistry that are almost identical in different acetaldehyde chemistry models. Additionally, our recent studies [1,23] have found that the H-atom abstractions from acetaldehyde by CH_3O and CH_3O_2 radicals are quite important. As such, the rate coefficients and thermochemical parameters involved in the H-atom abstraction reactions from formaldehyde and acetaldehyde by CH_3O and CH_3O_2 radicals are updated following [1].

2.2. Sensitivity analysis

Brute force sensitivity analysis [27] is first conducted under the selected experimental conditions to obtain the kinetic and thermodynamic parameters that influence the model predictions. The conditions for sensitivity analysis are shown in Fig. 1, which covers the typical temperature and pressure conditions of interest to the combustion community.

Sensitivity analyses of kinetic parameters are performed by changing the pre-exponential factors of each reaction. The sensitivity coefficients are defined as $SC_i^A = \ln(\Delta\tau/\tau)/\ln(\Delta k/k)$, where $\Delta\tau$ is the simulated result after multiplying the original rate constant by 2, i.e., $\Delta k = 2 * k$, and τ is the original result. Sensitivity analyses are not conducted at fuel-rich conditions as the reactions from these conditions have already been identified from the sensitivity analyses at the stoichiometric and fuel-

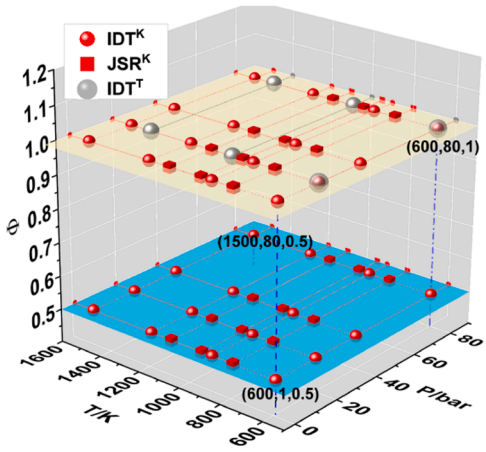

Fig. 1. The conditions for sensitivity analysis for kinetic parameters on IDT (red ball), kinetic parameters on JSR (red box), and thermodynamic parameters on IDT (gray ball).

lean conditions. Three species are selected in the sensitivity analysis of JSR experiments, namely CH_3CHO, CH_2O, and CO, which are key intermediates during the initial and later oxidation stages of acetaldehyde. For sensitivity analysis of ignition delay times, the ignition delay times in the simulations are defined as the time interval from the arrival of the shock wave at the end-plate or start of compression for RCM data to the maximum pressure rise (i.e., the onset of autoignition).

Sensitivity analyses of thermodynamic parameters are conducted following the method proposed by Lehn et al. [28]. The normalized sensitivity coefficients of ignition delay time on heat capacities are calculated via Eq. (1)

$$SC_i^{c_p} = \frac{\partial ln\tau_{ig}}{\partial lnc_{p,i}} = \frac{\tau_{ig}^{mod} - \tau_{ig}^{ori}}{\tau_{ig}^{ori}} \frac{1}{SAF_i - 1} \tag{1}$$

The heat capacity is modified by multiplying the polynomial coefficients with the sensitivity analysis factor, SAF_i, so that

$$a_{i,j}^{mod} = SAF_i * a_{i,j}^{ori},\ j = 1, 2, \ldots, 5 \tag{2}$$

where SAF_i is the sensitivity analysis factor of species i. Since the sensitivity is desired with respect to heat capacity only, the coefficients $a_{i,6}$ *and* $a_{i,7}$ have to be adapted as well to ensure that $\Delta h_{f,i}^{mod}(298\ K) = \Delta h_{f,i}^{ori}(298\ K)$ and $s_i^{mod}(298\ K) = s_i^{ori}(298\ K)$. As such, the sensitivity coefficients for enthalpies and standard entropies are defined as

$$SC_i^h = \frac{\partial ln\tau_{ig}}{\partial ln\left(exp\frac{\Delta h_{f,i}(298K)}{R \cdot 298K}\right)} = \frac{\tau_{ig}^{mod} - \tau_{ig}^{ori}}{\tau_{ig}^{ori}} \frac{R \cdot 298K}{\delta \Delta h_{f,i}} \tag{3}$$

$$SC_i^s = \frac{\partial ln\tau_{ig}}{\partial ln\left(exp\frac{s_i^0(298K)}{R}\right)} = \frac{\tau_{ig}^{mod} - \tau_{ig}^{ori}}{\tau_{ig}^{ori}} \frac{R}{\delta s_i^0} \tag{4}$$

where $\delta \Delta h_{f,i}$ and δs_i^0 are the absolute value of $\Delta h_{f,i}(298K)$ and $s_i^0(298K)$, respectively, $a_{i,6}$ and $a_{i,7}$ are increased in the brute-force method.

The 20 most sensitive reactions and species are selected from each condition, from which a total of 79 reactions and 24 species are obtained. Results of the sensitivity analyses are reported in the Supplementary Material (SMM) 2 & 3.

2.3. Statistical treatment of parameters

For each sensitive reaction, direct measurements and theoretical determinations of the rate coefficients in both reverse and forward directions are collected from the NIST Chemical Kinetics Database [29] and review articles [30–35]. The reverse rates are then converted into forward rates based on chemical equilibrium calculations using the thermodynamic properties of the species involved. When re-evaluating the rate coefficients, the data that were determined a long time ago and showed a large difference from recent experiments and quantum chemistry computations are excluded. While most data selected are from studies after 1990, a few data before 1990 are still considered because their overall trends are consistent with those of the more recent data.

For elementary reactions containing a third body, the low-pressure limiting rate is reevaluated. The adopted direct experiments and quantum chemistry computations, as well as the reevaluation process and the reevaluated rate parameters are summarized in SMM 4. If the corresponding data are utilized for the determination of the uncertainty range, the NIST ID is set in bold. The fitting process during kinetic parameter reevaluation is briefly described herein.

Three Arrhenius parameters (namely A, n and Ea) are reevaluated for all selected reactions using least squares curve fitting over the temperature range of 300 – 2500 K, assuming that the accuracy of all used data is consistent. In one case (R83, $HO_2+HO_2=H_2O_2+O_2$), six Arrhenius parameters (i.e., duplicated reactions) are used. The temperature dependence of rate coefficient k is described by the modified Arrhenius equation $k(T) = A\{T\}^n \exp(-Ea/RT)$, and the linearized form of which is

$$\kappa(T) = \alpha + nln\{T\} - \varepsilon T^{-1} = \theta^T p \tag{5}$$

where $\kappa(T) = \ln\{k(T)\}$ represents the logarithm of the rate coefficient, $\alpha = \ln\{A\}$, $\varepsilon = Ea/R$, $\theta = \left(1,\ lnT,\ -T^{-1}\right)^T$, and $p = (\alpha, n, \varepsilon)^T$ is the set of transformed Arrhenius parameters. The equation for the least squares fitting is defined as

$$F(T;\tilde{\mathbf{x}}) = \tilde{\alpha} + \tilde{n}ln\{T\} - \tilde{\varepsilon}T^{-1} \tag{6}$$

where the vector $\tilde{\boldsymbol{x}} = (\tilde{\alpha},\ \tilde{n},\ \tilde{\varepsilon})$ represents the Arrhenius parameters that need to be reevaluated. The optimization objective function during the fitting process is described as

$$\Phi(\boldsymbol{x}^*) = \sum_{m=1}^{N} (\kappa(T_m) - F(T;\tilde{\boldsymbol{x}}))^2 \tag{7}$$

where $\boldsymbol{x}^*$ is the optimal parameter set that minimizes the deviation between the fitted rate coefficient and the original data; N is the number of temperature conditions used for re-fitting Arrhenius parameters; T_m is the actual temperature for experimental measurements and theoretical calculations, $T_m \in [300,\ 2500]K$; and $\kappa(T_m)$ is the logarithm of the corresponding rate coefficient, as determined from Eq. (5).

For each sensitive species, the mean value of $\Delta h_f(298\ K)$ is determined from reported data that are available in the Active Thermochemical Tables (ATCT) [36], the NIST Chemistry WebBook [29], and the Third Millennium Thermodynamic Database (TMTD) [37]. For four species (namely CH_3CO_3, $HOCH_2O$, CH_3CO_3H, and O_2CH_2CHO), no thermochemical information can be found in the above databases. On the other hand, the literature data for $s^0(298\ K)$ and c_p are much more lacking. Therefore, $s^0(298\ K)$ and c_p for all species, and the $\Delta h_f(298\ K)$ for the four species are reevaluated based on 35 published chemical kinetic models for C_2—C_5 hydrocarbons, following the method proposed in [38]. Thereafter, the NASA polynomials for the 24 species are modified based on the reevaluated $\Delta h_f(298\ K)$, $s^0(298\ K)$, and c_p. The reevaluated thermochemical parameters and 35 published mechanisms are summarized in SMM 3, while the modification of thermochemical parameters via the NASA polynomials is briefly discussed herein.

For heat capacity, c_p, the NASA coefficients a_1-a_7 are revised via Eqs. (8)–(10):

$$a_{i,j}^{new} = a_{i,j}^{ori} * \frac{c_p^{mean}}{c_p^{ori}},\ j = 1, 2...5 \tag{8}$$

$$a_{i,6}^{new} = T\left(1 - \frac{c_p^{mean}}{c_p^{ori}}\right)\left(a_{i,1}^{ori} + \frac{1}{2}a_{i,2}^{ori}T + \frac{1}{3}a_{i,3}^{ori} + \frac{1}{4}a_{i,4}^{ori}T^3 + \frac{1}{5}a_{i,5}^{ori}T^4\right) + a_{i,6}^{ori} \tag{9}$$

$$a_{i,7}^{new} = \left(1 - \frac{c_p^{mean}}{c_p^{ori}}\right)\left(a_{i,1}^{ori}lnT + a_{i,2}^{ori}T + \frac{1}{2}a_{i,3}^{ori}T^2 + \frac{1}{3}a_{i,4}^{ori}T^3 + \frac{1}{4}a_{i,5}^{ori}T^4\right) + a_{i,7}^{ori} \tag{10}$$

For enthalpy, Δh_f(298 K), the coefficients a_6 is revised via Eq. (11):

$$\overline{a_{i,6}^{new}} = a_{i,6}^{new} + \frac{\left(\Delta h_f(298\text{K})^{mean} - \Delta h_f(298\text{K})^{ori}\right)}{R} \tag{11}$$

For entropy, s^0(298 K), the coefficients a_7 is revised via Eq. (12):

$$\overline{a_{i,7}^{new}} = a_{i,7}^{new} + \frac{\left(s^0(298\text{K})^{mean} - s^0(298\text{K})^{ori}\right)}{R} \tag{12}$$

where c_p^{mean}, $\Delta h_f(298\text{K})^{mean}$, $s^0(298\text{K})^{mean}$ are the mean values of

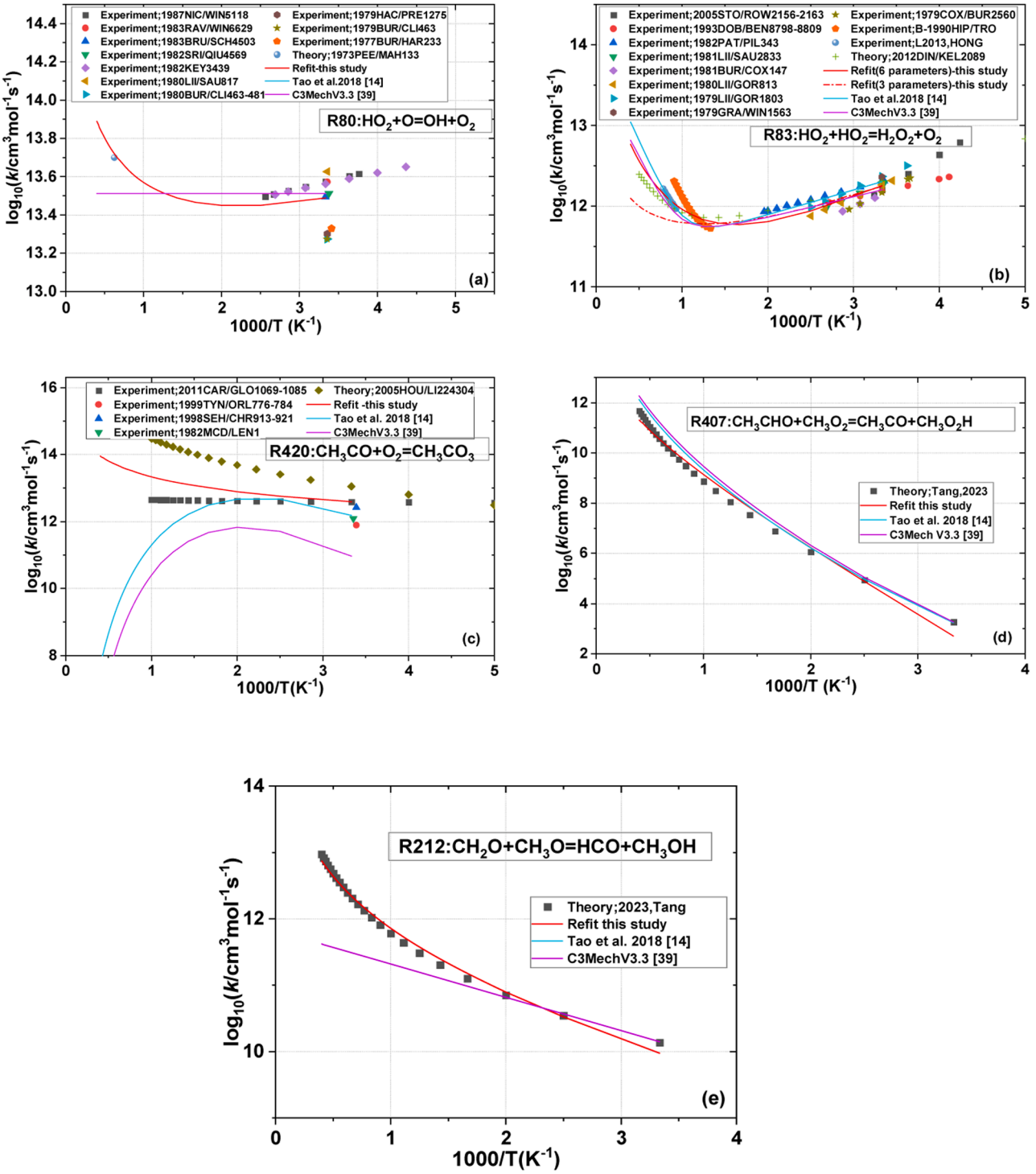

Fig. 2. The reevaluated rate coefficients for (a)R80, (b)R83, (c)R420, (d)R407, and (e)R212 (thick red line), along with the values adopted by Tao et al. [14] (thick blue line), C3MechV3.3 [39] (thick purple line), and all data used for refitting (symbols).

Δh_f(298 K), s^0(298 K), and c_p, respectively. $a_{i,j}^{new}$, $\overline{a_{i,6}^{new}}$, $\overline{a_{i,7}^{new}}$ are the revised NASA polynomial coefficients.

3. Results and discussion

3.1. Reevaluation of the rate parameters

Fig. 2 illustrates the reevaluated rate coefficients for R80: HO_2+O═$OH+O_2$, R83: HO_2+HO_2═$H_2O_2+O_2$, R420 CH_3CO+O_2═CH_3CO_3, R212: CH_2O+CH_3O═$HCO+CH_3OH$, and R407: $CH_3CHO+CH_3O_2$═$CH_3CO+CH_3O_2H$, along with the rate coefficients adopted in Tao et al. [14] and C3MechV3.3 [39], as well as the direct and theoretical data from literature. The results for all other reactions are summarized in SMM 4. For R80, as shown in Fig. 2a, Tao et al. [14] and C3MechV3.3 [39] suggested that the rate coefficient is constant over 300 - 2500 K. However, based on the experimental measurements from Keyser [40] and Peeters [41], the rate coefficient exhibits moderate and non-monotonic temperature dependence. This temperature dependence is better captured by the reevaluated rate coefficient from this study. For R83 (Fig. 2b), the single Arrhenius expression shows poor performance in replicating the data points in the high-temperature region. As such, the rate coefficients are refitted using double Arrhenius expression (i.e., six parameters), where much better agreement with the experimental data is achieved. It can be seen from Fig. 2b that the reevaluated rate coefficient differs slightly from those adopted in Tao et al. [14] and C3MechV3.3 [39], with smaller curvature on the high temperature end. For R420 (Fig. 2c), the reevaluated rate coefficient differs considerably from the recommendation from Tao et al. [14] and C3MechV3.3 [39], both quantitatively and qualitatively. The reevaluated rate coefficient clearly achieves a better representation of the experimental data. In fact, the trend observed with R420 has been found to be quite common among the 79 reactions analyzed, showing that it is necessary to reevaluate k for all important elementary reactions based on direct experiments and theoretical values from quantum chemistry computations. Additionally, for R407 (Fig. 2d) and R212 (Fig. 2e), as well as several other reactions, the rate data is very limited, and only the theoretical data that were recently calculated by Tang et al. [1] can be found. Nevertheless, obvious from Fig. 2d and e is the discrepancies between the calculated rate by Tang et al. [1] and those recommended by Tao et al. [14] and C3MechV3.3 [39]. A better agreement is achieved by the refitted rate coefficients, particularly at high temperatures that are more important to combustion modeling.

3.2. Reevaluation of the thermochemical parameters

Table 1 summarizes the thermochemical properties (c_p(298 K), Δh_f(298 K), and s^0(298 K)) of the 24 selected species computed from Tao et al. [14] and reevaluated in this study. It can be seen in Table 1 that there are significant differences in the heat capacity and entropy of CH_3O, the enthalpy and heat capacity of CH_3O_2, the heat capacity of CH_3O_2H, and the enthalpy of CH_2CHO, while the thermochemical properties of other species show relatively small changes.

3.3. Model validation and comparison

The reevaluated kinetic and thermodynamic properties based on direct experiments and theoretical calculations for the 79 reactions and 24 species, respectively, are incorporated into the original model (i.e., that proposed by Tao et al. [14]), which is further used to simulate the available fundamental combustion experiments. The updated model is included in SMM 5 & 6. To assess the predictive capability of the reevaluated model, available fundamental experiments from the literature are adopted for model validation and other published acetaldehyde chemistry models (Wako et al. [17], Hashemi et al. [16], Tao et al. [14], Zhang et al. [13], Mevel et al. [11]) are also included for comparison. As summarized in Tables 2, 3, the experiments cover 123 shock tube and 10 RCM ignition measurements over T = 800 - 1750 K, P = 2.03 - 9.87 atm and Φ = 0.5 - 2.5, 633 JSR species concentration data over T = 460 - 1230 K, P = 0.921 - 10 atm and Φ = 0.43 - 4, and 102 flow reactor species concentration data over T = 450 - 900 K, P = 25 bar, and Φ = 0.49. The wide coverage of the thermodynamic and fuel loading conditions should be sufficient to test the reevaluated model.

It is important to note that a major objective of this study is to determine the uncertainty domain for acetaldehyde thermochemistry for the optimization work that is currently in progress in the authors' group. Due to the limited experimental and theoretical data on thermodynamic properties for the species identified in this study, it is

Table 1
Species selected for optimization, the thermochemical properties parameters (c_p(298 K), Δh_f(298 K), and s^0(298 K)) in the initial mechanism and the reevaluated values of the parameters.

Species	Δh_f(298 K) / kcal/mol·K			c_p(298 K) / cal/mol·K			s^0(298 K) / cal/mol·K		
	Tao et al.	This study	absolute change	Tao et al.	This study	absolute change	Tao et al.	This study	absolute change
CH_3OH	−48.04	−48.02	0.02	10.26	10.33	0.07	57.52	57.41	0.11
H_2O_2	−32.48	−32.36	0.12	10.14	10.21	0.07	56.06	55.94	0.12
CH_3	35.06	35.01	0.05	9.18	9.20	0.02	46.37	46.37	0
CH_4	−17.83	−17.81	0.02	8.53	8.51	0.02	44.54	44.53	0.01
HOCHO	−90.48	−90.46	0.02	9.87	10.14	0.27	59.07	59.17	0.1
HO_2	2.94	2.94	0	8.34	8.34	0	54.76	54.76	0
CH_3CHO	−39.72	−39.57	0.15	13.22	13.16	0.06	63.08	63.08	0
CH_3O	5.05	5.15	0.1	10.23	9.82	0.41	54.91	55.65	0.74
CH_3O_2	2.74	3.12	0.38	11.62	12.42	0.8	64.36	64.43	0.07
CH_3CO	−2.46	−2.40	0.06	12.14	12.22	0.08	63.90	63.90	0
CH_2CO	−11.52	−11.57	0.05	12.19	12.18	0.01	57.66	57.79	0.13
CH_3O_2H	−30.39	−30.52	0.13	14.16	15.79	1.63	65.97	65.81	0.16
CH_3OCH_3	−43.84	−43.98	0.14	15.39	15.56	0.17	63.90	63.85	0.05
OH	8.92	8.91	0.01	7.14	7.09	0.05	43.91	43.91	0
C_2H_5	28.92	28.44	0.48	59.08	59.17	0.09	12.01	11.92	0.09
CH_2CHO	3.05	3.88	0.83	12.99	12.97	0.02	63.14	62.82	0.32
HCO	10.11	10.11	0	8.29	8.30	0.01	53.60	53.62	0.02
CO	−26.42	−26.42	0	6.96	6.95	0.01	47.24	47.24	0
H	52.10	52.10	0	4.97	4.97	0	27.42	27.40	0.02
H_2O	−57.79	−57.80	0.01	8.03	8.02	0.01	45.13	45.12	0.01
CH_3CO_3	−42.35	−42.36	0.01	19.91	19.85	0.06	77.73	77.49	0.24
$HOCH_2O$	−42.16	−42.02	0.14	13.04	13.04	0	66.11	65.93	0.18
CH_3CO_3H	−80.49	−80.49	0	20.48	20.48	0	77.24	77.20	0.04
O_2CH_2CHO	−21.01	−21.01	0	17.28	17.28	0	79.98	79.98	0

Table 2
Summary of shock tube and rapid compression machine data used for model validation and comparison.

P (atm)	T(K)	Φ	Mole fraction			No. of data points	Refs.
			CH_3CHO	O_2	Ar		
3.45	1295–1538	0.5	0.005	0.025	0.97	6	
3.45	1368–1487	1.0	0.0086	0.0214	0.97	7	[11]
3.45	1337–1579	1.5	0.0112	0.0188	0.97	10	
2.03	1275–1619	0.5	0.01	0.05	0.94	17	
2.06	1275–1619	1.0	0.02	0.05	0.93	17	[10]
2.32	1399–1704	2.5	0.02	0.02	0.96	9	
10	734–1086	1.0	0.0278	0.0692	0.903	10	[14]
3.50	1315–1598	0.5	0.005	0.025	0.97	9	
3.50	1365–1735	2.0	0.01	0.0125	0.9775	12	
5.00	1272–1516	0.5	0.005	0.025	0.97	13	[8]
5.00	1275–1532	0.5	0.01	0.05	0.94	11	
5.00	1250–1477	1.0	0.01	0.025	0.965	12	

deemed appropriate to use the recently published mechanisms for this purpose, though that the mechanisms published later might contain better, revised thermodynamics data for the identified species in Table 1. Simulations are first conducted to evaluate the impact of the updated kinetic parameters, the updated thermodynamic parameters, and both on the model performance, with the results summarized in Figs. 3 and 4. It is clear from Figs. 3 and 4 that the change in model performance is dictated by the updates to the kinetic parameters, while the updates to the thermodynamic parameters exhibit minor impact. Nevertheless, their influences can become quite significant in other uncharted conditions, as can be inferred from the magnitude of the sensitivity analysis results on thermodynamic properties in SMM 3. Therefore, all possible sources of uncertainty in the acetaldehyde chemistry are considered. This gives better model uncertainty presentation and provides better flexibility for the optimization of acetaldehyde chemistry in our future studies. Specifically, updating the kinetic parameters promotes the ignition and oxidation reactivity of the acetaldehyde model, while further updating the thermodynamic parameters slightly promotes the ignition reactivity at the low temperature end of the temperature range investigated in Fig. 3.

Figs. 5–10 show the simulated results and the experimental measurements at several representative conditions, while the validation and comparison results at other conditions are summarized in SMM 1. It can be seen from Fig. 5 that, by incorporating the reevaluated rate and thermodynamic parameters, the model becomes more reactive, leading to smaller simulated ignition delay times at all conditions investigated. The temperature dependence of autoignition reactivity seems to be unaffected by the model updates. Similar trends are also seen in Figs. S4–S6, where the updated model and other existing models are compared against shock tube ignition measurements within the high-temperature regime. Overall, the updates incorporated in the model yield a satisfactory prediction and an improved agreement compared to other chemistry models for the ignition delay times measured in shock tubes at temperatures between 1250 and 1700 K.

Fig. 6 further demonstrates the comparison results of different models for predicting the ignition delay times of acetaldehyde in the low- to intermediate-temperature regimes (i.e., 734 – 1086 K, as shown in Table 2) in an RCM [14]. As can be seen from Fig. 6, the qualitative agreements between the models and the experiments differ greatly from those observed within the high-temperature regimes (e.g., Fig. 5). The models from Tao et al. [14] and Hashemi et al. [16] are in better agreement with the experimental data, while the models from this study and Wako et al. [17] are poor, which is the opposite to the trends observed in Fig. 5. Specifically, the models from this study tend to overpredict the ignition delay times at temperatures below 920 K, while greatly underpredicting the ignition delay times at temperature above 1000 K. The reason for this is not immediately clear and are discussed

Table 3
Summary of jet-stirred reactor data used for model validation and comparison.

Residence time (s)	P(atm)	T(K)	Φ	Mole fraction				Data points	Refs.
				CH_3CHO	O_2	N_2	Ar		
0.8	10	929–1085	0.43	0.00129	0.0075	0.99121	–	35	
0.08	1	1008–1227	0.82	0.00123	0.00375	0.99502	–	44	[8]
0.8	10	959–1176	1	0.0015	0.00375	0.99475	–	45	
0.08	1	1057–1167	1.61	0.00197	0.00186	0.99617	–	51	
3–6	0.934	461–816	0.5	0.02	0.1	0.88	–	49	
3–6	0.947	490–894	1	0.02	0.05	0.93	–	80	[13]
3–6	0.947	560–890	4	0.02	0.0125	0.9675	–	81	
3	0.921	528–946	0.5	0.025	0.125	–	0.85	248	[15]

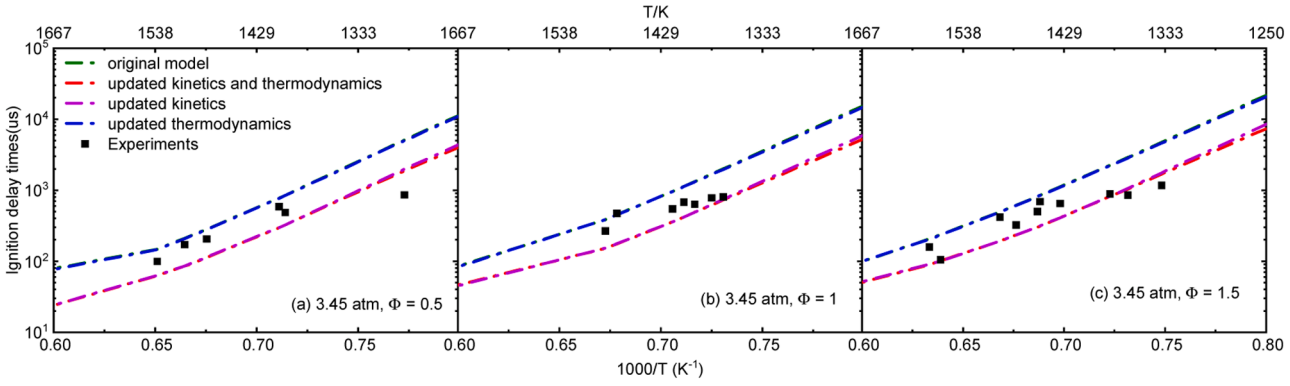

Fig. 3. Comparison between measured (symbols) and simulated (lines) ignition delay times for $CH_3CHO/O_2/N_2$ mixtures in a shock tube. (a) $P = 3.45$ atm, $\Phi = 0.5$, 0.5 % CH_3CHO / 2.5 % O_2 / 97 % Ar. (b) $P = 3.45$ atm, $\Phi = 1.0$, 0.86 % CH_3CHO / 2.14 % O_2 / 97 % Ar. (c) $P = 3.45$ atm, $\Phi = 0.5$, 1.12 % CH_3CHO / 1.88 % O_2 / 97 % Ar. Experimental data are taken from [11].

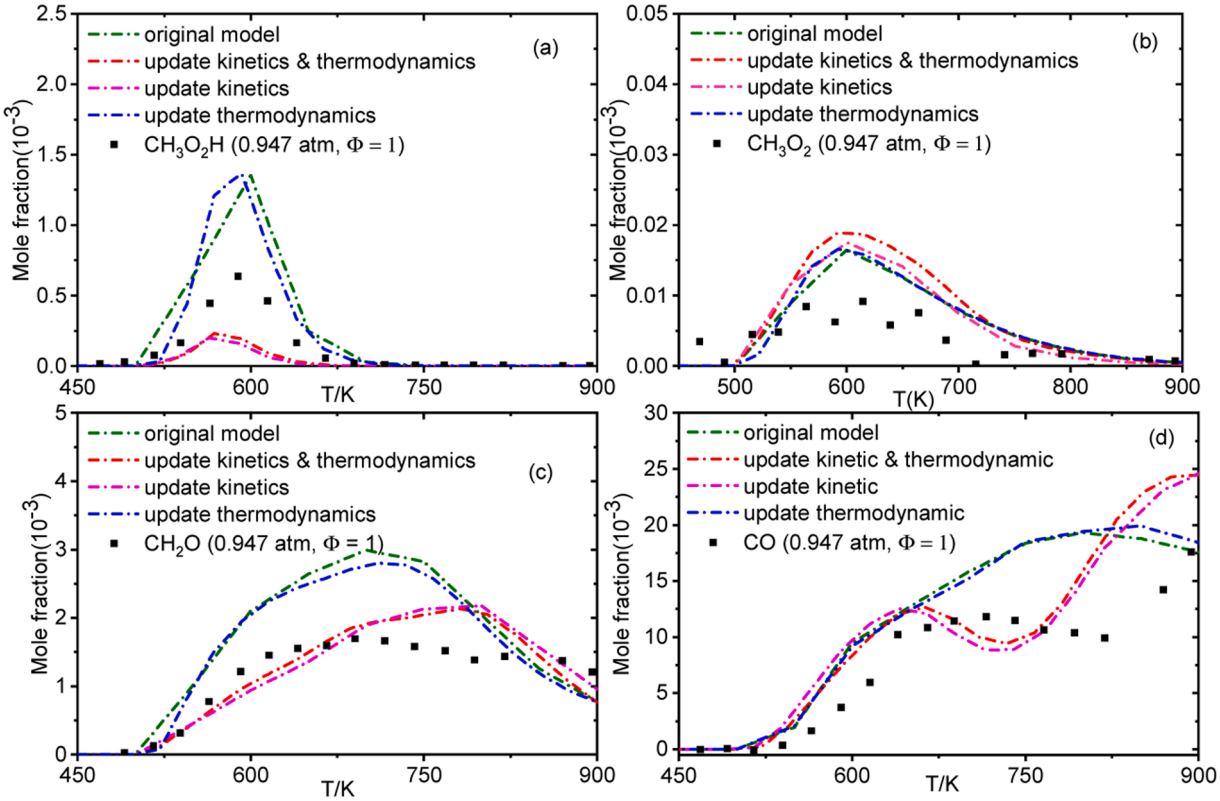

Fig. 4. Comparison between measured (symbols) and simulated (lines) species profiles (CH_3O_2H, CH_3O_2, CH_2O, CO) during the oxidation of CH_3CHO in a JSR at P = 0.947 atm, Φ = 1.0, 2 % CH_3CHO / 5 % O_2 / 93 % N_2. Experimental data are taken from [8].

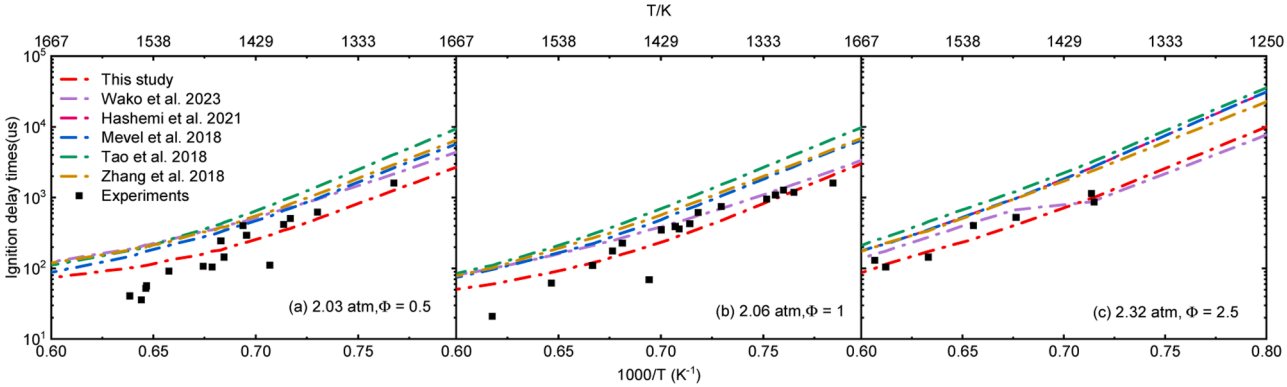

Fig. 5. Comparison between measured (symbols) and simulated (lines) ignition delay times for CH_3CHO/O_2-Ar mixtures in a shock tube. Experiment data are taken from [10] and simulation results are obtained using the model from this study, Wako et al. [17], Hashemi et al. [16], Zhang et al. [13], Mevel et al. [11], and Tao et al. [14].

further in Section 3.4.

The model from this study and other studies are further compared against measured species profiles during the acetaldehyde oxidation in a JSR at P = 0.947 atm, Φ = 1 and 4, and low temperatures. The temperature range covered by the JSR experiments in [13] (approximately 460 – 890 K, as summarized in Table 3) is even lower than those investigated in [14] in the RCM (i.e., Fig. 6). As shown in Fig. 7, at stoichiometric condition, the updated model shows modestly improved prediction accuracy of the mole fractions of the major products (e.g., CH_2O, CH_3OH and CO) at temperatures between 450 and 700 K than the other models. At most conditions under 700 K, the update model performs similar to the original model [14] except for CH_3O_2H and CH_2O, where the original model overpredicts the production of CH_3O_2H and CH_2O, while the updated model underpredicts their production. Above this temperature, the simulated species profiles from the updated and original model deviate greatly from each other where the oxidation reactivity of acetaldehyde in the updated model is significantly lower than the original model. These changes in model reactivity agree with those observed in Fig. 6, where the ignition reactivity also becomes smaller in the updated model. Also seen in Fig. 7 is the enhanced NTC behavior of CO predicted by the updated model, which leads to somewhat better agreement with the experiments in comparison to the original model. On the other hand, the predictions of acetaldehyde consumption from the updated model in the NTC region do not exhibit better agreement with the experiments than the original model.

At fuel-rich condition (i.e., Φ = 4, Fig. 8), the updated model becomes more reactive than the original model at temperatures above 750 K. As can be seen from Fig. 8a, the updated model overestimates the

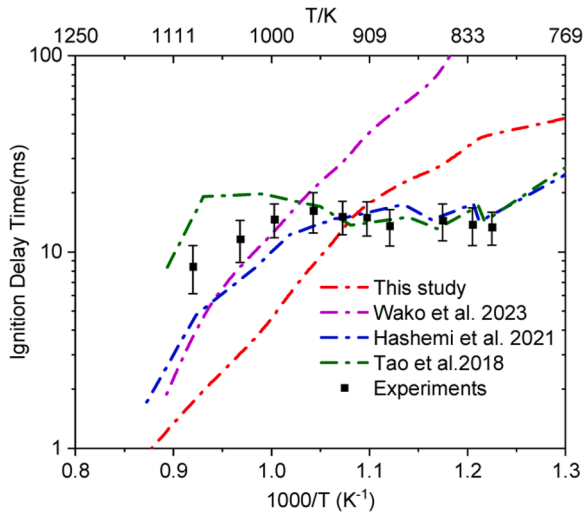

Fig. 6. Comparisons of acetaldehyde ignition delay times in RCM at 10 bar, Φ = 1, and dilution ratio of 13 between measurements from Tao et al. [15] and simulation results using the model from this study, Wako et al. [17], Hashemi et al. [16], and Tao et al. [14]. Symbols: experimental data. Lines: modelling results.

acetaldehyde oxidation reactivity, showing significantly higher acetaldehyde consumption rate, hence an over predicted carbon monoxide mole fraction (Fig. 8f), as compared to the experiments and the original model.

Fig. 9 show the comparison between the measured and simulated species profiles during acetaldehyde oxidation in a JSR at $P = 700$ Torr and $\Phi = 0.5$. As can be seen from Fig. 9, the updated model underpredicts CH_3CHO consumption at temperatures above 600 K, as compared to the original model, leading to a lower agreement with the experiment measurements. However, the NTC behavior of CO_2 (Fig. 9g) and CH_2O (Fig. 9d) predicted by the updated model in this study is enhanced with better agreement with experiments achieved. Fig. 10 further demonstrates the comparison between measured (symbols) and simulated (lines) species profiles during the oxidation of CH_3CHO in a flow reactor at $P = 25$ bar. As shown in Fig. 10, the updated model predictions are in good agreement with experiments, except for CO_2, C_2H_6, and CH_4. Specifically, the updated model overpredicts the production of CO_2, and underpredicts the production rates of C_2H_6 and CH_4 at above 750 K. Overall, the updated model is comparable to the original model.

The overall model performance is further evaluated with more detailed and specific comparisons against all experimental measurements with respect to different types of experiments and with respect to different species for JSR experiments. Fig. 11 illustrates the relative differences between the shock tube measurements and the model predictions from various models at different pressure conditions. The experimental data are taken as the values of the original measurements. At temperatures below 1500 K, the differences between all models are more pronounced. It is clear from Fig. 11 that at all pressure conditions, the updated model outperforms all other models in capturing the high-temperature shock tube experiments, with the best improvement observed at 2.03 – 2.32 atm (Fig. 11a). The improved model accuracy slightly diminishes as pressure is increase to 5 atm.

Figs. 12 and 13, further illustrate the comparison of accuracy between different models against capturing the JSR measurements. The peaks in the curves are a result of using lines to connect all data points for relative differences (temperatures from low to high), without distinguishing between equivalence ratios and pressures. Overall, the updated model demonstrates a comparable performance in comparison to all other models. Although significant discrepancies are observed in Figs. 7 and 8 for CH_3CHO and CO at temperatures above 750 K (which is greater than those observed for the other models), the overall agreement averaged over all JSR measurements become similar among all models for these two species.

It is interesting to see that although the updated model is not adjusted against these fundamental experiments (i.e., all the important reactions and species are reevaluated based on direct experiments and theoretical calculations for rate and thermodynamic parameters), it yields a satisfactory performance in replicating all the fundamental experiments (except for the RCM measurements as shown in Fig. 6), which is overall equivalent to the other models. At some conditions, the model even outperforms (e.g., Figs. 11–13) the other models that have already been calibrated based on the reported experiments. This highlights the validity of physics-based reevaluation of the model parameters using direct experiments and high-level theoretical computations.

Nevertheless, the insufficient performance of the updated model in capturing the RCM measurements is still concerning. This implies that the kinetic parameters for some low- to intermediate-temperature reactions are not properly determined in the updated acetaldehyde model. For instance, the refitted rate coefficient for R80 ($HO_2+O = OH+O_2$) in Fig. 2a at the range of 1000 K/$T = 1$ - 2.5 exhibits a curvature that differs from the that adopted in the original model. This is reasonable for determining the representative uncertainty domain of this reaction (as discussed in the following), while might cause significant changes in model predictions. However, the results in Figs. 14–16 indicate that R80 is not among the most sensitive reactions at 750 – 1150 K for both oxidation and ignition process, ruling out this reaction as the major reason for the discrepancies observed between the updated and original models. As shown in Fig. 2c, for R420 ($CH_3CO+O_2 = CH_3CO_3$), the reevaluated rate coefficient differs considerably from the recommendation from Tao et al. [14] and C3MechV3.3 [39], which is re-evaluated to be higher than the original value in the temperature range 300–2500K. To quantify the impact of the updated rate coefficient for R420 on model performance, ignition delay time simulations are performed at two experimental conditions using four different models: (1) the updated model; (2) the updated model but with retaining the original rate coefficient of R420; (3) the original model from Tao et al. [14]; and (4) the original model but with adopting the updated rate coefficient of R420. The comparison results are summarized in Fig. S22. As shown in Fig. S22, the change in rate coefficient for this reaction is not influential, and that the differences between the original and updated models in predicting the RCM measurements are not caused by this reaction.

On the other hand, many changes are applied to reactions and thermochemistry that are relevant to the high and low temperature C_0–C_2 sub-chemistries in the updated model (as can be seen from SMM 4). These changes should also be validated against experimental measurements directly for the C_0–C_2 species, to ensure that these kinetic and thermodynamic parameters are not over-tuned. As such, validations of the updated model against shock tube and JSR experiments have also been performed. The comparison results, along with other models (i.e., Wako et al. [17], Hashemi et al. [16], Mevel et al. [11], Tao et al. [14], and Zhang et al. [13]), are summarized in Figs. S15–S17 in SMM 1 for methane [42] and hydrogen [43]. As can been seen from Figs. S15–S17, the updated model performs either comparable or better than other models in capturing the ignition characteristics of these smaller species at some conditions. However, the updated model overpredicts ignition delay times of hydrogen at $P = 4$ and 10 atm, Φ=1, temperatures of 900 – 1000K. On the other hand, as can be seen from Fig. S17, at 900 – 1000 K, the updated model performs either comparable or better than the other models in predicting the mole fractions of O_2, H_2, and H_2O. Closer examination of the results in Fig. S15 and Fig S16 in SMM 1 indicates that the original model is among the worst for predicting methane autoignition while demonstrating reasonable agreement for predicting hydrogen autoignition. These inconsistencies in the original model, as well as the discrepancies of the updated model between the hydrogen autoignition and JSR modelling results all highlight the poorly represented acetaldehyde chemistry in existing models. Also, as can be seen

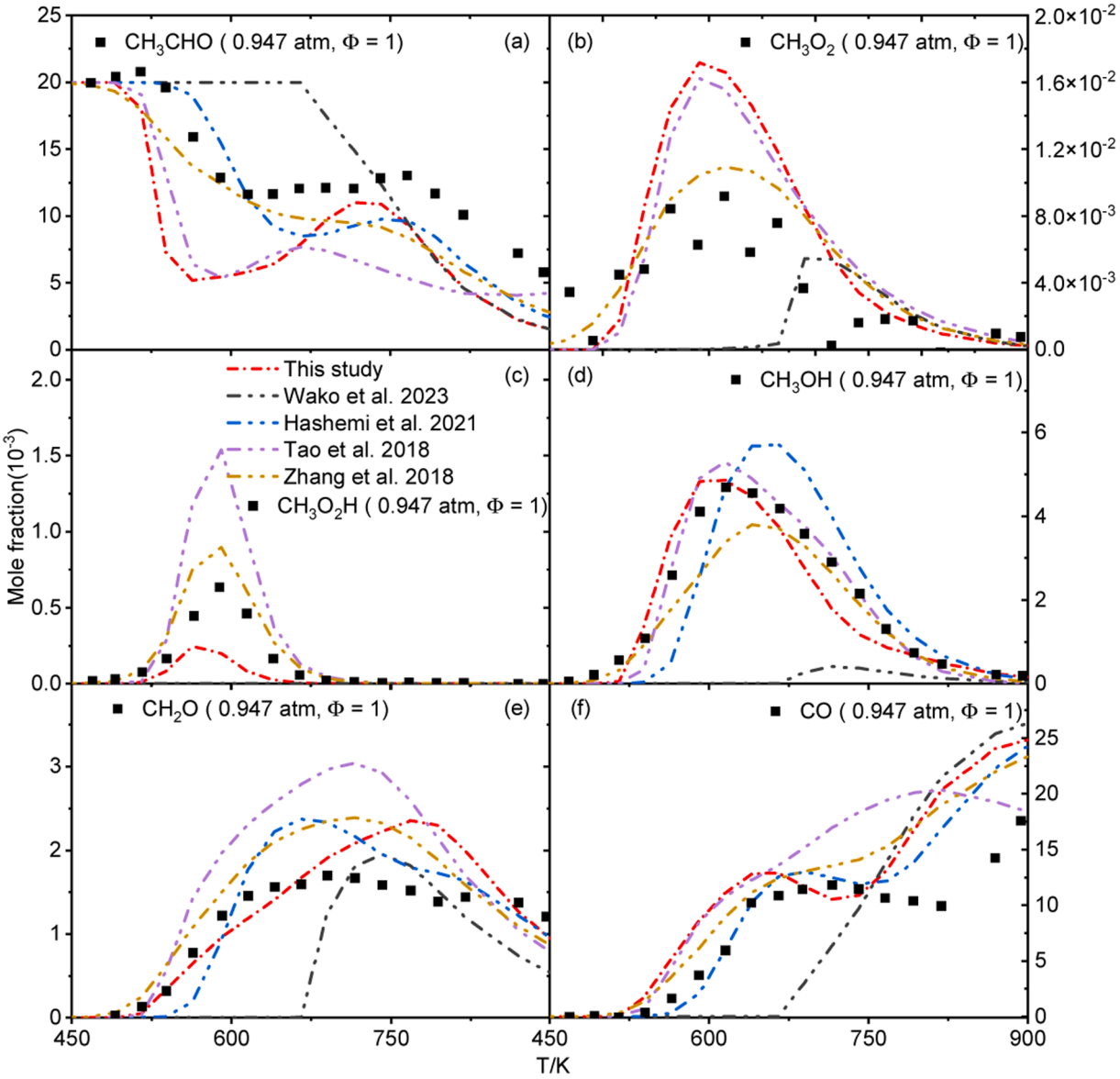

Fig. 7. Comparison between measured (symbols) and simulated (lines) species profiles during the oxidation of CH_3CHO in a JSR at P = 0.947 atm and Φ = 1. Experimental data are taken from [13] and simulation results are obtained using the model from this study, Wako et al. [17], Hashemi et al. [16], Zhang et al. [13], and Tao et al. [14].

from Figs. 12 and 13, the updated model shows overall comparable agreement with the JSR measurements over 750 – 1100 K, whereas performs poor in capturing the RCM measurements in the same temperature range (c.f., Fig. 6). These inconsistent trends are likely caused by more than one reaction, which can be non-trivial to address. This, however, does not affect the major purpose of this study, which is to determine the physical uncertainty domains of all key kinetic and thermodynamic parameters. On the contrary, the results obtained from this study enable further model uncertainty quantification and optimization (with a case demonstrated in the following) that have been proved to be quite powerful to address the observed discrepancies. In fact, a forthcoming study is currently in progress in the authors' group, where all experimental measurements used for model validation are included for model optimization, where the poor agreements between the updated model and the RCM measurements will be addressed.

3.4. Sensitivity and flux analyses

To explore the underlying kinetics that lead to the changes in model performance, sensitivity analysis is performed at T = 750 and 1150 K for the ignition delay time of a stoichiometric acetaldehyde mixture at P = 10 bar, using both the original model from Tao et al. [14] and the updated model. The sensitivity analysis results are shown in Fig. 14, covering the top 20 most sensitive reactions. At T = 750 K, the sensitivity coefficients computed by the original model and the updated model are significantly different, with almost all the promoting and inhibiting reactions exhibiting stronger contributions to autoignition reactivity. The promoting effect from the top promoting reaction, i.e., $CH_3CO+O_2 = CH_3CO_3$, is enhanced by approximately 70 %. This is expected as the rate coefficient of this reaction has been increased considerably in the updated model, as shown in Fig. 2c. At T = 1150 K, as shown in Fig. 14b, most reactions have similar sensitivities between the updated and original models. However, the sensitivity of the most inhibiting reaction in the original model, namely R99 ($CH_3+HO_2 = CH_4+O_2$), is reduced by more than half, and the sensitivity of the most promoting reaction ($CH_3CHO+HO_2 = CH_3CO+H_2O_2$) is increased by around 100 %. These changes will lead to an increased model reactivity. This, again, agrees well with the trends seen in Fig. 5 and Figs. S4–S6 in

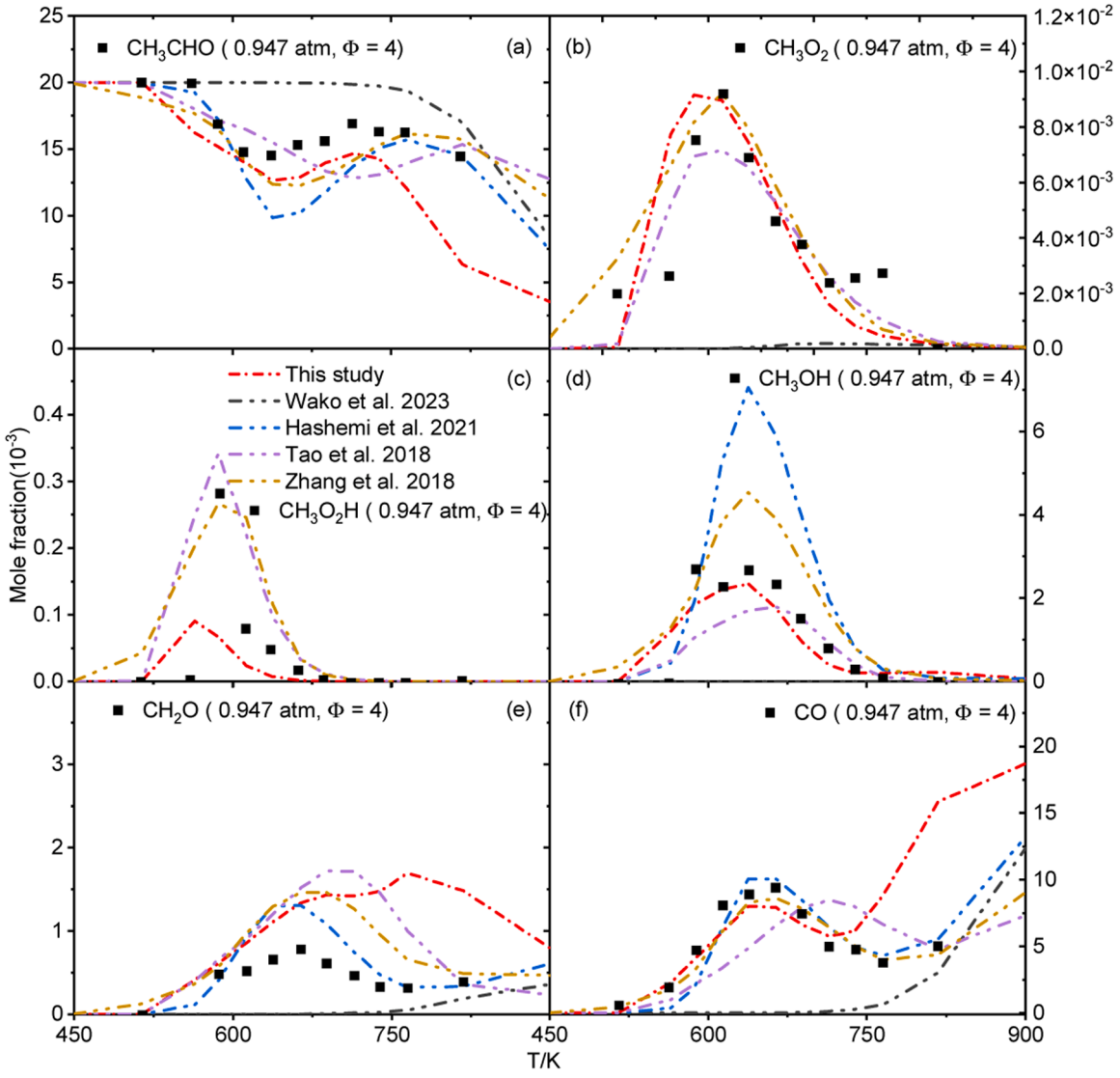

Fig. 8. Comparison between measured (symbols) and simulated (lines) species profiles during the oxidation of CH_3CHO in a JSR at $P = 0.947$ atm and $\Phi = 4$. Experimental data are taken from [13] and simulation results are obtained using the model from this study, Wako et al. [17], Hashemi et al. [16], Zhang et al. [13], and Tao et al. [14].

SMM 1 where the updated model exhibits higher reactivity at 1150 K and high temperatures.

To explore the kinetics for the discrepancies in predicting the RCM measurements from Tao et al. [15] by the updated model in this study, sensitivity analysis is further conducted at $\Phi = 1$, $P = 10$ bar and $T = 850$ K, for simulated ignition delay times. The top 20 most sensitive reactions are shown in Fig. 15a. As can be seen from Fig. 15a, the sensitivity of the most sensitive reactions changed significantly, of which the rate coefficients of 19 reactions are re-evaluated in this study. The influences of these reactions on model predictions are first investigated by restoring the rate parameters for these 19 reactions to the values adopted in the original model, referred to as the "partially updated model". Simulations are then performed using the original, updated and the partially updated models, with the results summarized in Fig. 15b. It can be seen from Fig. 15b that the partially updated model become comparable with the original model, indicating that the differences between the original and the updated models in reproducing the RCM experiments are mainly caused by these reactions.

Therefore, further analysis is conducted to examine the differences between the original and refitted rate coefficients for these 19 reactions. The rate coefficients before and after re-evaluation are illustrated in Fig. S18 in SMM 4. As can be seen from Fig. S18, the difference between the original and refitted rate coefficients is large. Among the 19 reactions, 6 reactions are further identified and discussed due to their large sensitivity (as observed in Fig. 15a) and large changes in rate coefficients (as shown in Fig. S18), which are R99: $CH_3+HO_2=CH_4+O_2$, R156: $CH_3O_2+CH_3=CH_3O+CH_3O$, R399: $CH_3CHO+OH=CH_3CO+H_2O$, R400: $CH_3CHO+OH=CH_2CHO+H_2O$, R404: $CH_3CHO+CH_3=CH_2CHO+CH_4$, and R440: $CH_2CHO=CH_3+CO$. For R99, the sensitivity of this reaction is reduced by >5 times in the updated model. As shown in Fig. 3a of SMM4, the rate coefficient in the original model replicates those proposed by Hong et al. [44] and Ryu et al. [45] while differing from those measured by Shaw [46] and Skinner et al. [47] by approximately one order of magnitude. The refitted rate coefficient from this study, on the other hand, is lowered by considering the measurements from Shaw [46] and Skinner et al. [47]. For R156, the sensitivity is reversed in the updated model (from a promoting reaction to an inhibiting reaction, as shown in Fig. 15a). As seen in Fig. S27a of SMM4, the rate coefficient adopted in the original model is based on the rate coefficients reported by Keiffer et al. [48] following a linear trend. However, the rate coefficients at room temperature reported in other studies Parkes [49] and Pilling et al. [50] are slightly

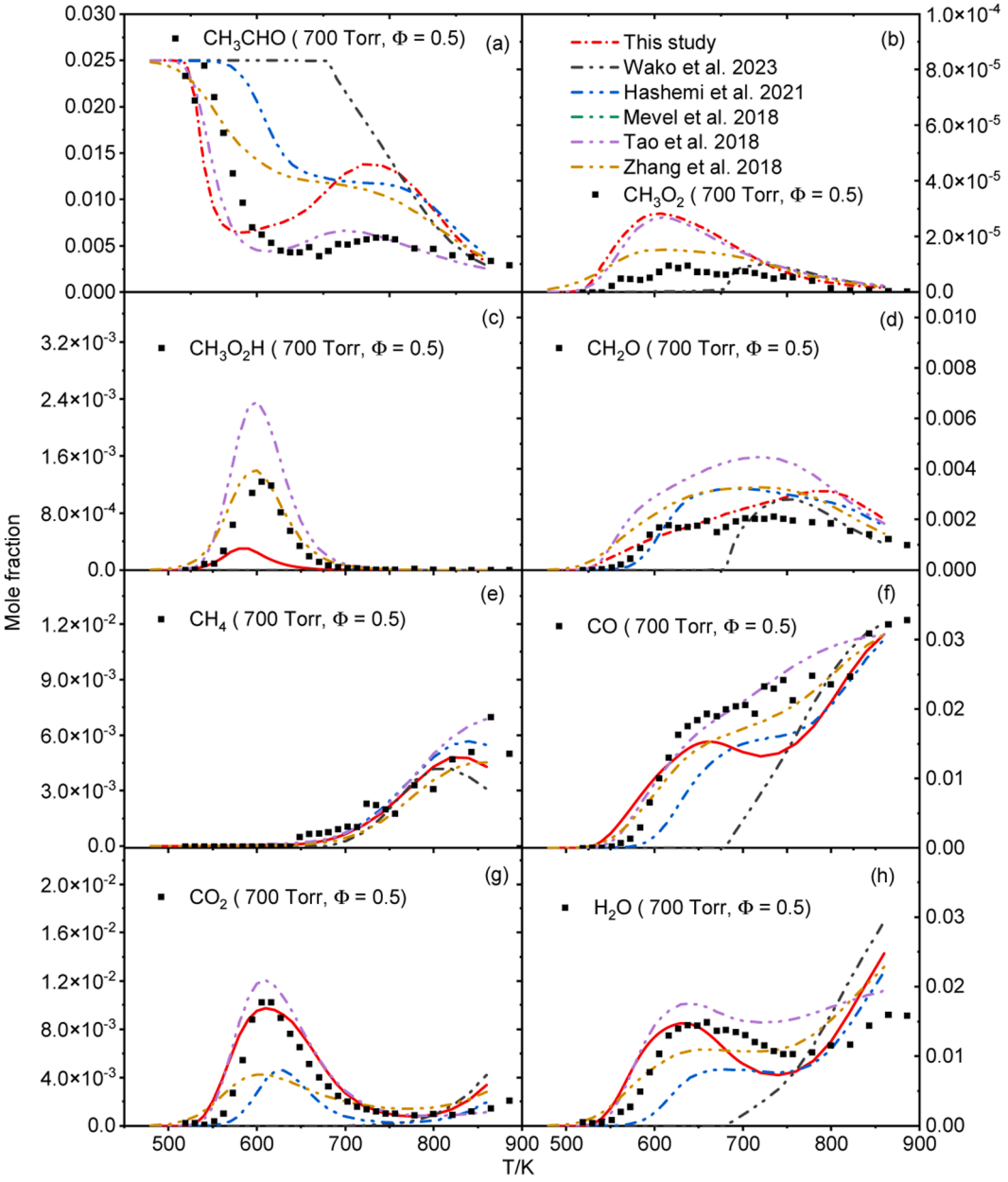

Fig. 9. Comparison between measured (symbols) and simulated (lines) species profiles during the oxidation of CH_3CHO in a JSR at $P = 700$ Torr and $\Phi = 0.5$. Experimental data are taken from [15] and simulation results are obtained using the model from this study, Wako et al. [17], Hashemi et al. [16], Zhang et al. [13], and Tao et al. [14].

lower than that adopted in the original model. To better capture the rate coefficient uncertainty at this temperature, the refitting shifted the rate coefficient to slightly lower values. For R404, the influence of this reaction on the model reactivity is insignificant, as can be seen in Fig. 15a, while in the updated model, it becomes the 4th most promoting reaction on ignition reactivity. The results in Fig. S30a in SMM4 indicates that the refitted rate coefficient replicates excellently the values reported by Yasunaga et al. [10], which is much better than that used in the original model. As this is the only study that investigated this reaction, the refitted values are considered more reliable than the original ones. For R399, the inhibiting effect of this reaction is almost tripled after refitting (c.f., Fig. 15a). The results in Fig. 10a of SMM4 indicate that the refitted rate coefficient overlap that adopted by Dong et al. [39], which represent better the available experiments and computations [51–53] than that adopted in the original model. It is also clear from Fig. 15a that the promoting effect of R400 is enhanced by more than two times. The refitting results in Fig. S29a of SMM4 indicate that the rate coefficient in the original model follows a linear trend, while that refitted in this study is slightly curved to better capture the temperature dependence of the rate coefficients reported by Yasunaga et al. [10]. Finally, for R440, which showed a significant change in rate coefficient after the refitting (as can be seen in Fig. S18a), the refitted rate coefficient achieves a considerably better representation of all available rate data than the original rate coefficient, as shown in Fig. 18a of SMM4.

The poor performance of the updated model in reproducing the RCM experiments and the large changes in rate coefficients after refitting highlight the limitations of using unrefined fittings over literature rates to assess acetaldehyde chemistry. Nevertheless, this does not affect the major purpose of this study, which is to assess the physically representative uncertainty of important rate parameters for subsequent optimization. Additionally, each reaction has also been restored individually to examine if the changes in model performance for RCM simulations are

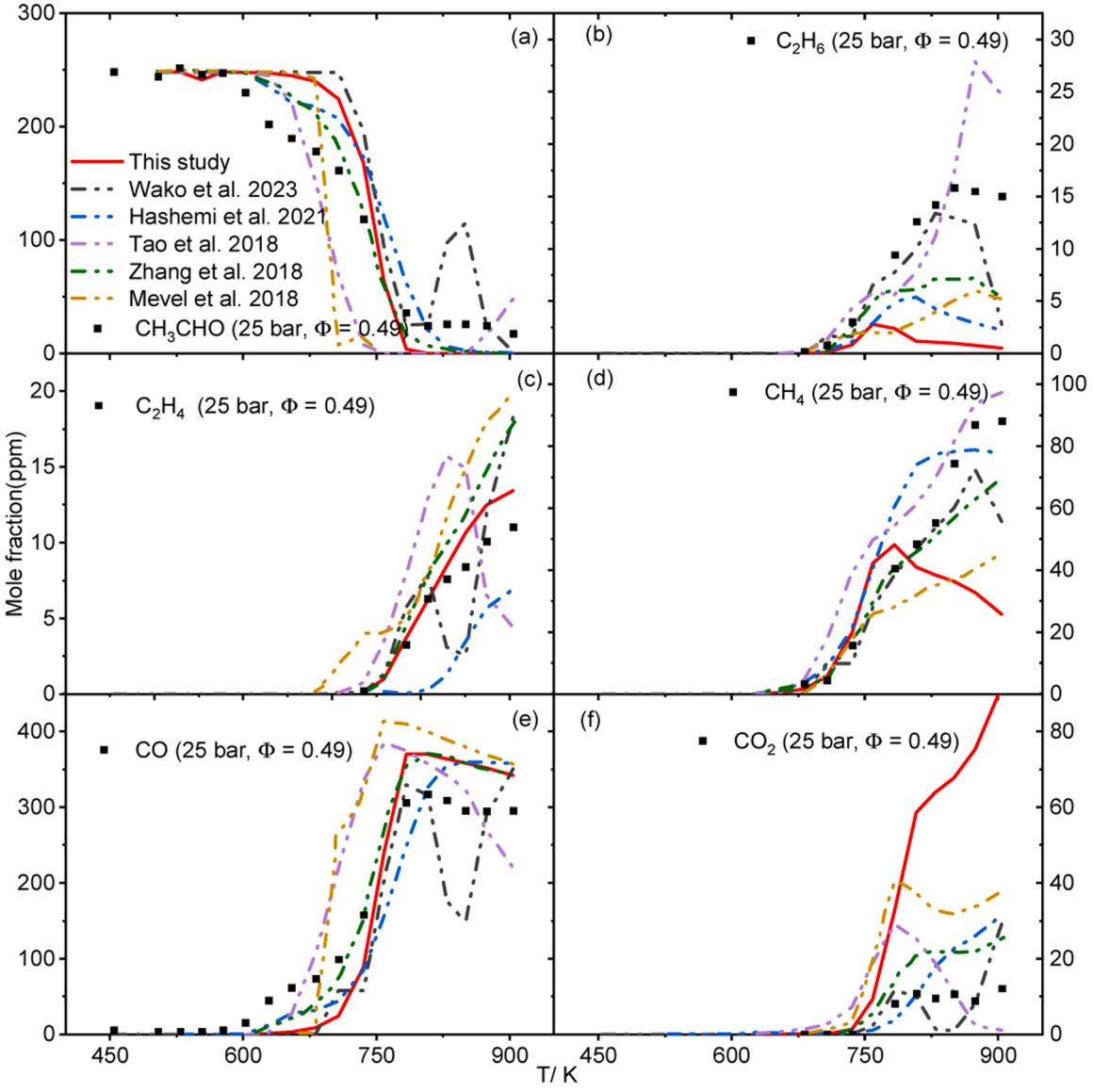

Fig. 10. Comparison between measured (symbols) and simulated (lines) species profiles during the oxidation of CH_3CHO in a flow reactor at $P = 25$ bar, 248 ppm of CH_3CHO, 1265 ppm of O_2, diluted in nitrogen ($\Phi = 0.49$). Experimental data are taken from [16] and simulation results are obtained using the model from this study, Wako et al. [17], Hashemi et al. [16], Mevel et al. [11], Tao et al. [14] and Zhang et al. [13].

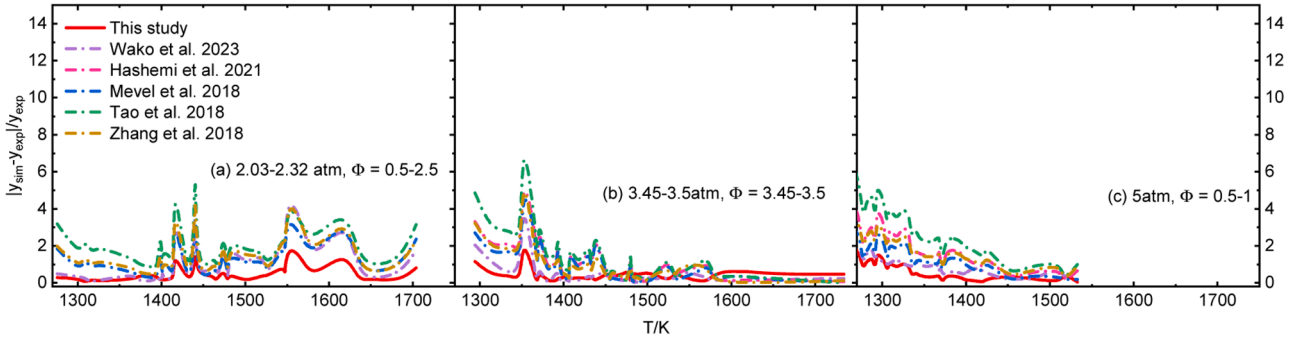

Fig. 11. Comparison of relative differences between experimental measurements [8,11,14] and model predictions from this study, Wako et al. [17], Hashemi et al. [16], Mevel et al. [11], Tao et al. [14], and Zhang et al. [13] for the ignition delay times in shock tubes at different pressures. The middle panel is plotted using the scale indicated on the left y axis.

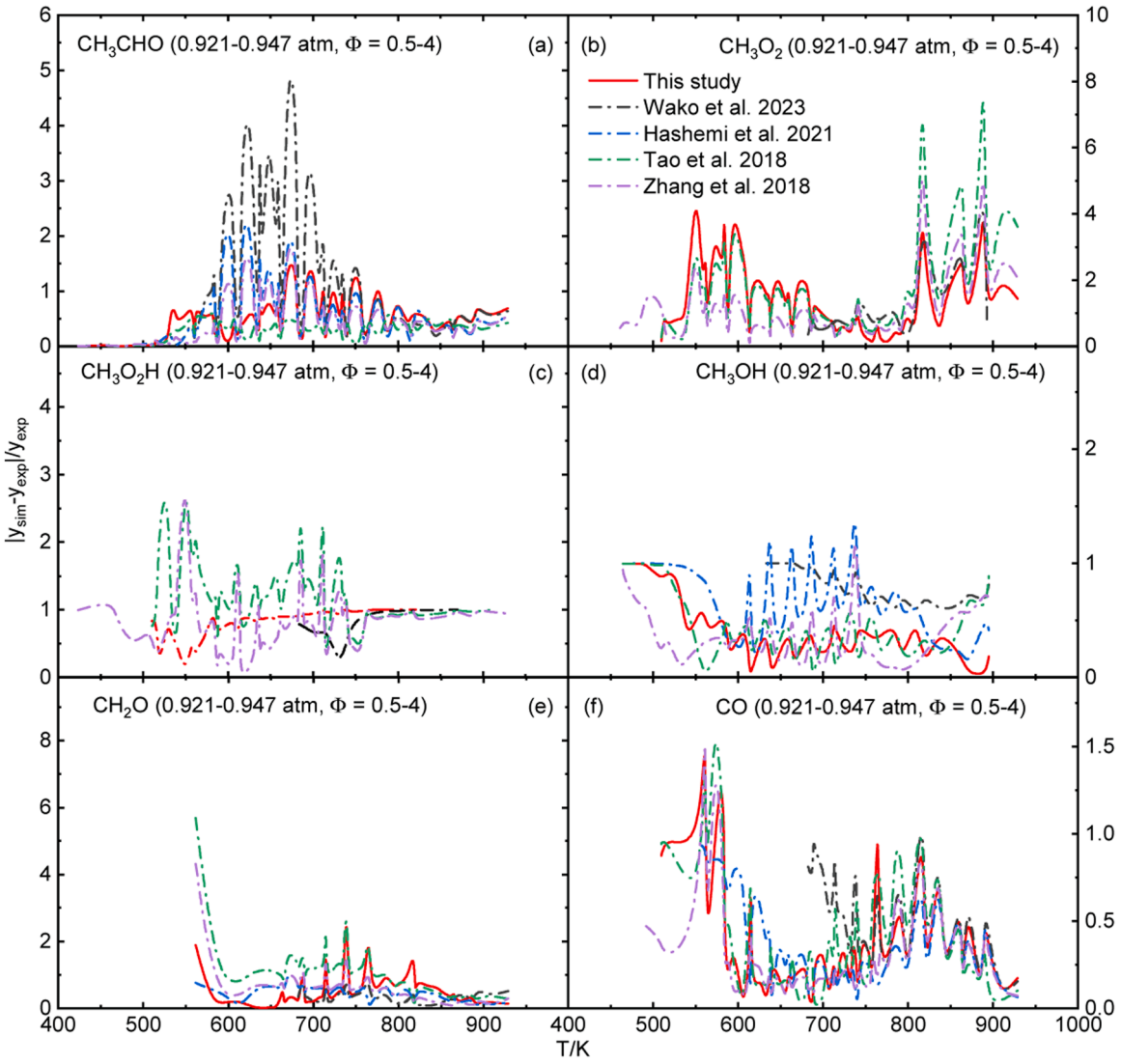

Fig. 12. Comparison of relative differences between experimental measurements [13,15] and model predictions from this study, Wako et al. [17], Hashemi et al. [16], Tao et al. [14], and Zhang et al. [13] for the species profiles during the oxidation of CH_3CHO in JSR at $P = 0.934 - 0.947$ atm.

caused by a single reaction. This is quickly ruled out as restoring a single reaction could not reproduce the modelling results from the original model. In fact, the refitting results discussed above and illustrated in SMM4 clearly demonstrate that a large portion of the identified reactions are not properly defined for their rate coefficients in the original model, e.g., R400 where the original rate coefficient differs considerably from that recently determined by Yasunaga et al. [10]. These discrepancies might be able to be cleared with manual adjustments of individual rate coefficients, but should be done in a holistic manner where all rate coefficients are optimized concurrently. Such optimization cannot be achieved or physically justified without a representative uncertainty domain, as discussed with Fig. 18 in Section 4.

Concerning the difference between the original and updated models, as well as between the updated model and the experiments in predicting the JSR experiments, a sensitivity analysis of acetaldehyde mole fraction using the original and updated model at $T = 800$ K and the same condition as in Fig. 8 is conducted. The results are summarized in Fig. 16, covering the top 20 most sensitive reactions. As can be seen from Fig. 16, the updated model exhibits larger negative sensitivity coefficients for most of the consumption reactions of acetaldehyde. Notably, the sensitivity of R401 ($CH_3CHO+HO_2 = CH_3CO+H_2O_2$), which is the most sensitive reaction promoting the consumption of acetaldehyde, has been increased by >5 times in the updated model. Additionally, the sensitivity of R254 ($CH_3+CH_3(+M) = C_2H_6(+M)$), which is the top inhibiting reaction in the original model for CH_3CHO consumption, has been decreased by >8 times. These changes result in the higher oxidation reactivity of CH_3CHO with the updated model, as observed in Fig. 8a. The increased consumption of CH_3CHO leads to the increased production of CH_2O and CO, as can be seen in Fig. 8e and f. Flux analysis is further conducted at the same conditions as in Fig. 8, with the results shown in Fig. S23 of SMM 1. As can be seen from Fig. S23, the flux through the $CH_3CHO+HO_2$ pathway is increased, while the flux through the $CH_3+CH_3(+M)$ pathway is decreased in the updated model, resulting in an increased importance of R401 ($CH_3CHO+HO_2$═$CH_3CO+H_2O_2$) and a decreased importance of R254 ($CH_3+CH_3(+M)$=$C_2H_6(+M)$) during acetaldehyde consumption. Observations of the refitting results in SMM4 (namely Fig. 7a for R401 and Fig. 4a for R254 in SMM 4) both indicate a better representation of the literature data by the refitted rate parameters. This is most obvious with R401 where the refitted rate coefficients agree excellently with the reported values from Altarawneh et al. [54] and Colket et al. [55].

For the discrepancies in predicting hydrogen ignition delay times by the updated model in this study (as shown in Fig. S16 of SMM 1), sensitivity analysis is further conducted at $\Phi = 1$, $P = 4$ atm, and $T = 1000$ K. The top 10 most sensitive reactions are shown in Fig. S21a, of

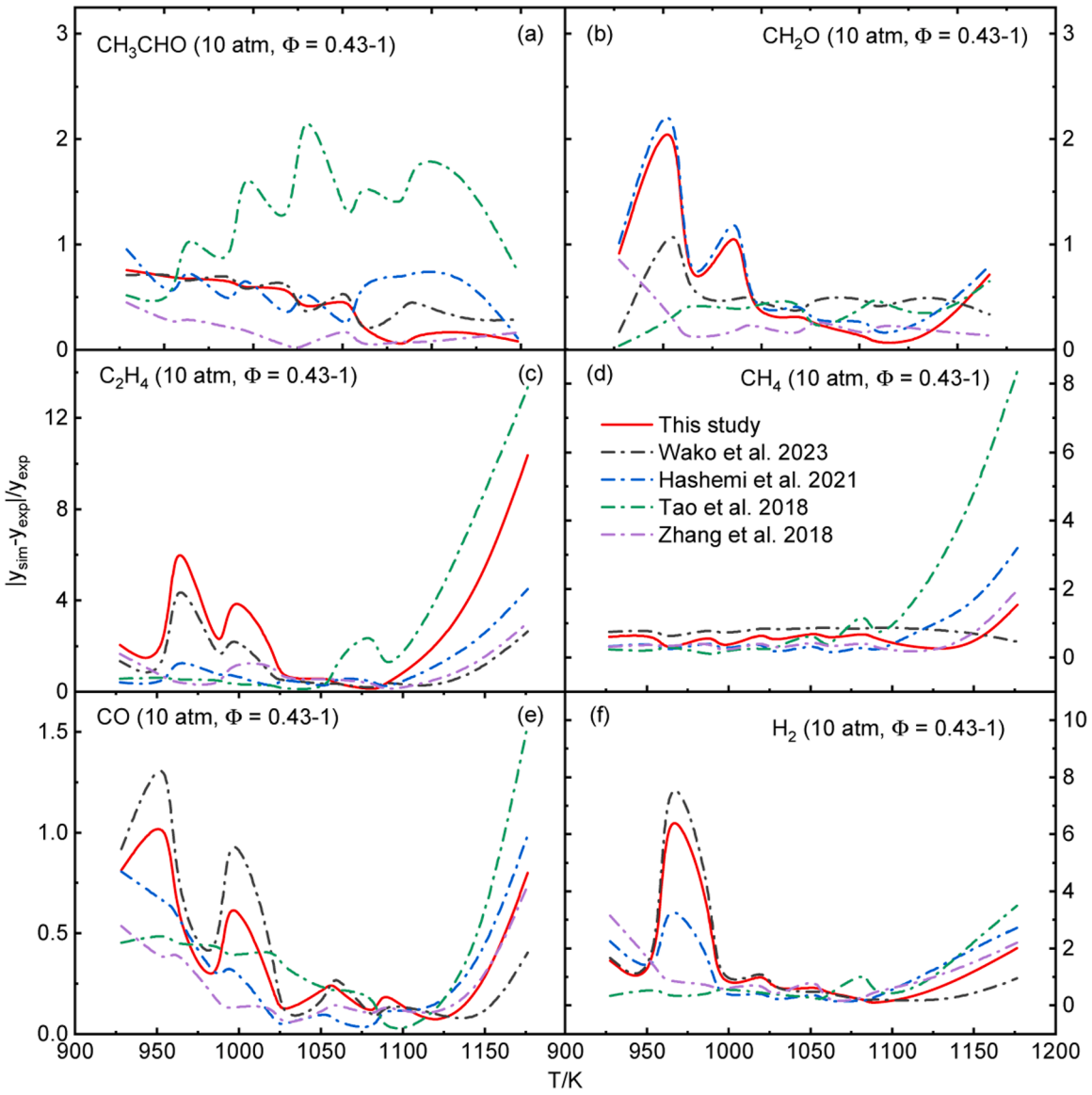

Fig. 13. Comparison of relative differences between experimental measurements [8] and model predictions from this study, Wako et al. [17], Hashemi et al. [16], Tao et al. [14], and Zhang et al. [13] for the species profiles during the oxidation of CH_3CHO in JSR at $P = 10$ atm.

which the rate coefficients of 9 reactions were re-evaluated in this study. Restoring the rate coefficients for these 9 reactions to the values in the original model shifted the prediction results to those predicted by the original model. The rate coefficients before and after refitting are also shown in Fig. S19. Based on the changes in sensitivities as shown in Fig. S21a and the changes in rate coefficients as shown in Fig. S19, 3 reactions are further analysed, which are R56: $O_2+H = O+OH$, R79: $HO_2+H = H_2+O_2$ and R85: $H + O_2(+M)=HO_2(+M)$. For R56, the promoting effect of this reaction on hydrogen ignition reactivity is lowered in the updated model. The change in sensitivity for this reaction is the greatest among all sensitive reactions at this condition. However, as can be seen from Fig. S19 h and Fig. S15a in SMM 4, the refitting does not lead to noticeable changes in the rate coefficient. There is only a slight shift on the low-temperature end, where the updated rate coefficient represents better all literature data. For R79, the inhibiting effect of this reaction is enhanced in the updated model, as can be seen from Fig. S21a. The rate coefficient of this reaction in the original model differs significantly from the existing literature, particularly at the low temperature end where large qualitative and quantitative disagreement can be seen, as shown in Fig. S1a in SMM 4. This indicates that this reaction is not well represented in the original model. On the other hand, the refitted rate coefficient represents better the qualitative trend and quantitative values of all reported rate data. Particularly, the rate coefficients reported by the most recent study (i.e., those computed by Mousavipour et al. in 2007 [56]) is well represented by the updated rate parameters. For R85, which is the top inhibiting reaction at this condition, the refitting increases the original rate coefficient by approximately 0.2 order of magnitude at all temperatures. The rate coefficient in the original model follows the measurements reported by Bates et al. [57] and Michael et al. [58] with Ar as the third body. This however deviates from the reported rate coefficients with N_2 as the third body. The updated rate coefficient, again, achieves a better representation of all available data, based on which the uncertainty range can be more accurately defined.

Flux analysis is further conducted at the same conditions as in Fig. 14 at the timing of 1 % CH_3CHO consumption. The results at $T = 750$ and 1150 K are shown in Fig. 17 and Fig. S25 in SMM 1, respectively. As shown in Fig. 17, significantly different branching ratios are observed at 750 K for the conversions from CH_3CHO to CH_3CO and CH_2CHO, as well as from CH_2O to HCO. Specifically, with the updated rates, the

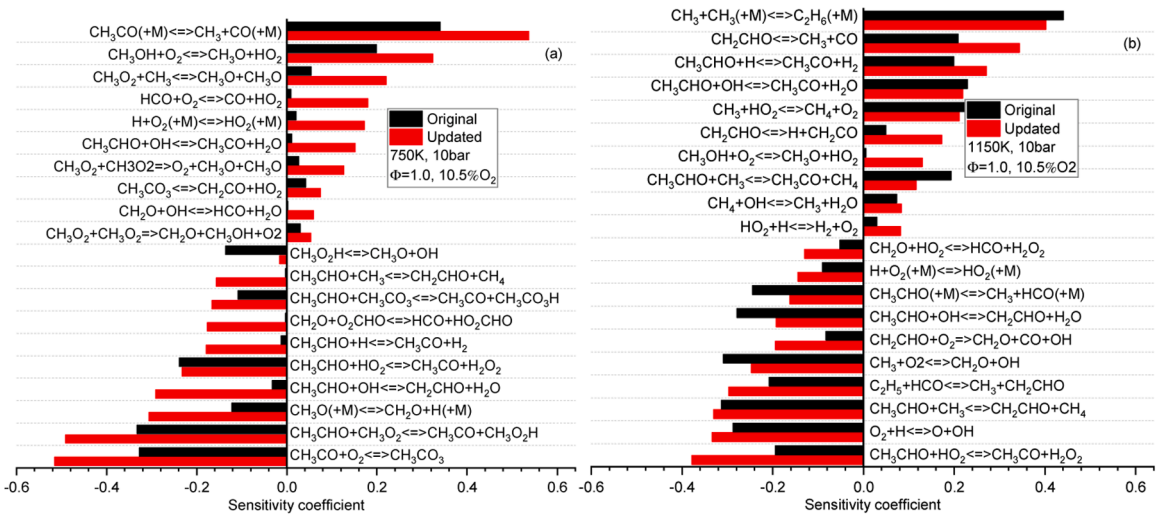

Fig. 14. Sensitivity analysis on ignition delay time for original and updated model at the diluted/stoichiometric condition, $P = 10$ bar and different temperatures; (a) $T = 750$ K and (b)1150 K.

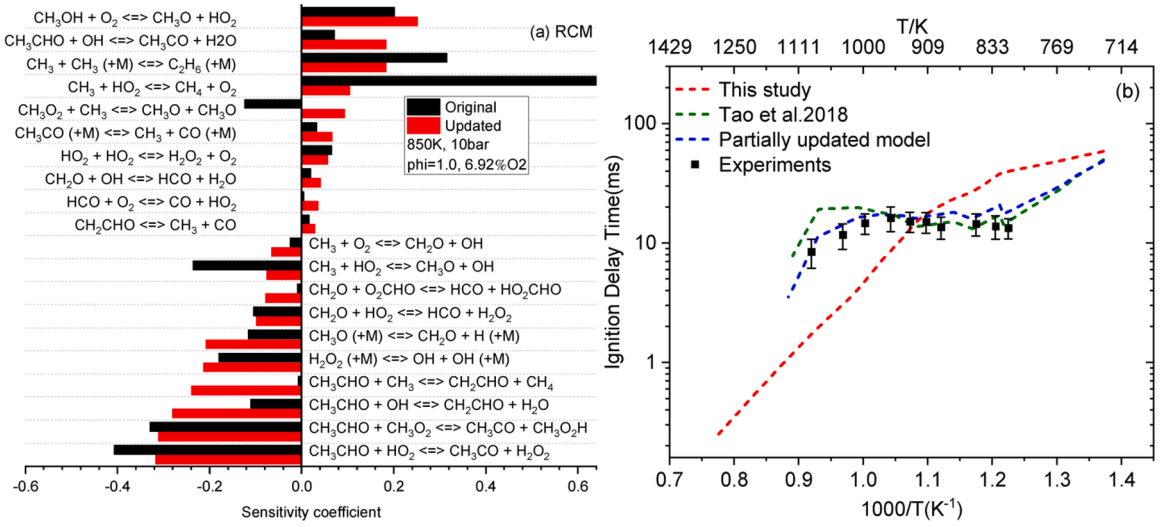

Fig. 15. (a) Sensitivity analysis on ignition delay time for original and updated model in RCM at $\Phi = 1$, $P = 10$ bar, and $T = 850$ K. (b) Comparisons of acetaldehyde ignition delay times in RCM at 10 bar, $\Phi = 1$, and dilution ratio of 13 between measurements from Tao et al. [14] and simulation results using the model from this study, Tao et al. [14], and the model from this study using the original rate coefficients for the 19 sensitive reactions . Symbols: experimental data. Dash lines: modelling results.

contribution of H-atom abstraction by OH radicals to CH_3HO consumption increases considerably, while that by CH_3O_2 radicals is suppressed. This is consistent with the SA results, where the sensitivity of CH_3CHO+OH pathways is increased by >10 times. There is also a clear shift toward the formation of CH_2CHO with the updated model (i.e., < 2.5 % and 27 % CH_3CHO is consumed to form CH_2CHO in the original and updated model, respectively). These CH_2CHO producing pathways promote reactivity, as can be seen in Fig. 14a. An increased flux via these pathways will lead to enhanced reactivity, supporting the shifted model reactivity as observed in Figs. S4–S13 in SMM 1. Additionally, a prominent rise and decrease is seen in the CH_2O consumption pathways by OH and CH_3O_2, respectively. Similar trends to those observed at 750 K are found at 1150 K (Fig. S25), with relatively smaller differences seen between the original and updated models.

4. Uncertainty analysis

As can been seen from Figs. 5–10, the disagreements between the updated model and the experiments are still significant, though slightly improved at high temperatures. These disagreements can be addressed by further optimizing the model parameters within the model uncertainty. Doing so, the model uncertainty needs to be defined with addressing two important questions: (a) is the parameter uncertainty rigorously defined based on known information? and (b) is the nominal parameter value a statistical representation of its uncertainty domain? Without properly addressing any of these information, the model uncertainty will be falsely conditioned, and thus empty solution will be returned when enough constraints have been applied during model optimization (e.g., data inconsistency) [59]. Fortunately, these two questions can now be addressed based on the updated chemistry model developed in this study, as the model parameters are evaluated purely based on direct experiments and quantum chemistry computations, which is a statistical representation of the respective parameter uncertainty domain. To this end, the uncertainties for the 79 reactions and the 24 species are evaluated in the following.

Firstly, the temperature-dependent uncertainty of the identified re-

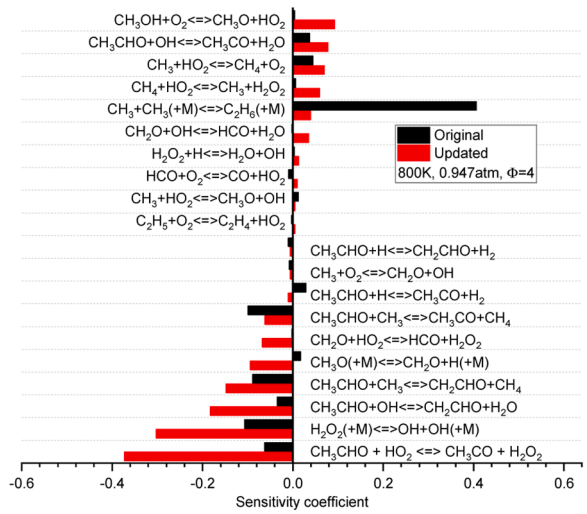

Fig. 16. Sensitivity analysis of CH_3CHO model fraction during acetaldehyde oxidation in a JSR at $\Phi = 4$, $P = 0.947$ atm, and $T = 800$ K.

actions is determined following the method proposed by Nagy and co-workers [60], while basing on the reevaluated reaction rates rather than the mean rate coefficients as adopted in [60]. The temperature-dependent uncertainty factor $f(T)$ are determined from the uncertainty bands $log_{10}(\kappa(T, \mathbf{x}^*)) \pm f(T)$, which are derived from the limiting values of the acceptable rate coefficients based on direct experiments, quantum chemistry computations, as well as the available review studies. The uncertainty factor determined in this study corresponds to 3σ deviations from the recommended values on a logarithmic scale, i.e., $\sigma_\kappa(T) = f(T)\cdot(ln10)/3$.

The relation between the variance of $\kappa(T)$ and the elements of the covariance matrix of the Arrhenius parameters is further obtained via the method proposed by Nagy et al. [60]:

$$\sigma_\kappa(T) = \sqrt{\Theta^T \Sigma_p \Theta} = \sqrt{\sigma_\alpha^2 + \sigma_n^2 ln^2 T + \sigma_\varepsilon^2 T^{-2} + 2r_{\alpha n}\sigma_\alpha\sigma_n lnT - 2r_{\alpha\varepsilon}\sigma_\alpha\sigma_\varepsilon T^{-1} - 2r_{n\varepsilon}\sigma_n\sigma_\varepsilon T^{-1} lnT} \quad (13)$$

where Σ_p is the covariance matrix of parameters (α, n, ε), $(\sigma_\alpha^2,\ \sigma_n^2,\ \sigma_\varepsilon^2)$ are variances, and $(r_{\alpha n},\ r_{\alpha\varepsilon},\ r_{n\varepsilon})$ are correlations. The covariance matrix Σ_p can be used to restore $f(T)$, which also defines the prior uncertainty domain of the Arrhenius parameters. The detailed derivation process for computing $\sigma_\kappa(T)$ is summarized in SMM 1. To determine the elements of the covariance matrix for the three-parameter Arrhenius expression, the uncertainty of the rate coefficient has to be known at least at six different temperatures [60]. This is achieved by determining the temperature points at every 100 K between [300, 2500] K, as shown in the inset in Fig. 18b.

For reactions involving third-bodies, additional treatment is needed to reconcile the data sources reported for different third bodies. In reevaluating the uncertainty for this type of reaction, the third-body collision efficiencies are pre-determined from literatures (see SMM 4) with that of N_2 set at unity and others set at different values relative to unity. An example is shown in Fig. 18 for R85: $H + O_2(+M) = HO_2(+M)$. It is clear from Fig. 18 that the reevaluated rate coefficient from this

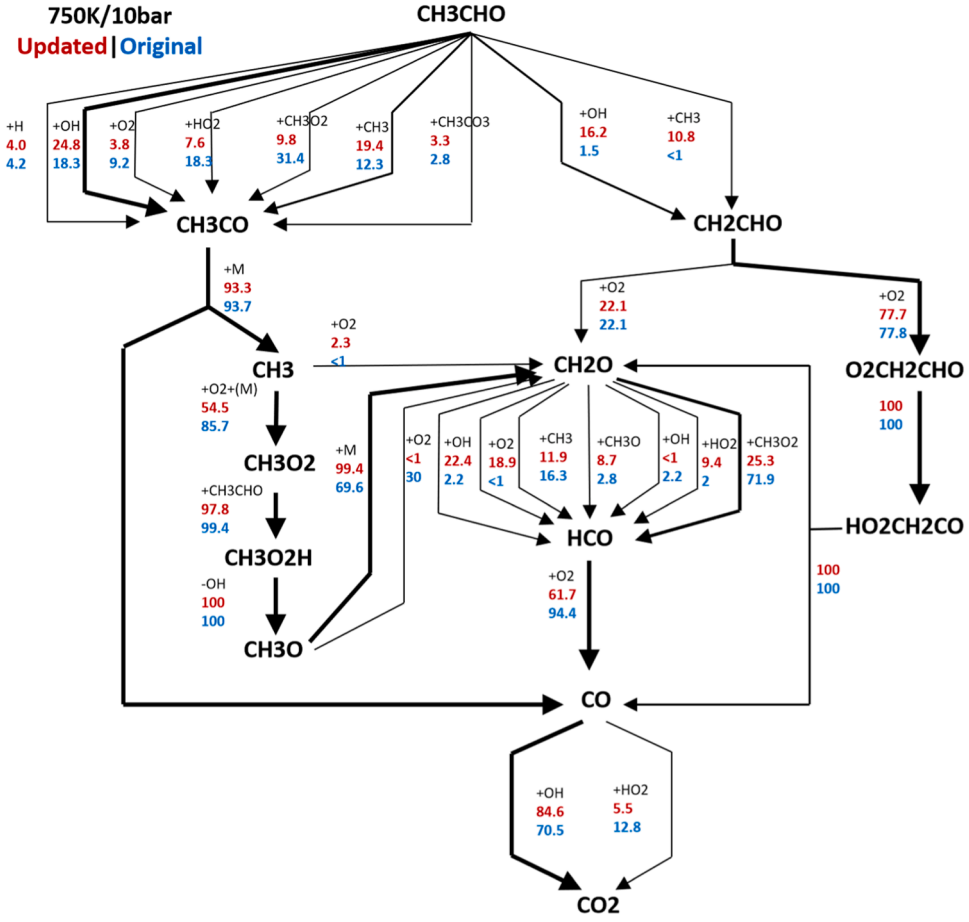

Fig. 17. Flux analysis at the timing of 1 % CH_3CHO consumption during ignition at stoichiometric condition, 10.5 % O_2 ratio, 750 K and 10 bar using the updated (red numbers) and original (blue numbers) model.

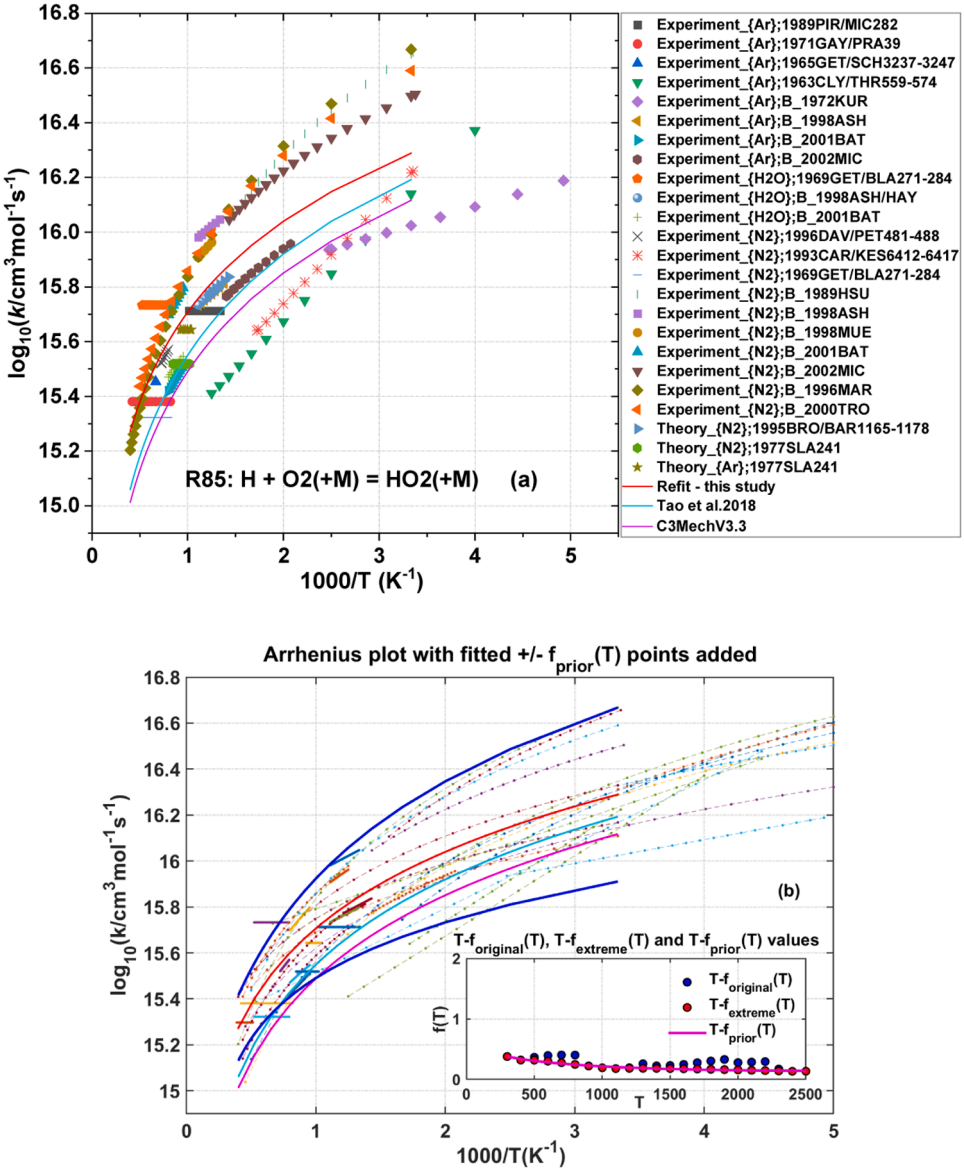

Fig. 18. (a) Reevaluated rate coefficients for R85 (symbols are labelled in the legend as *type of data {bath gases}: NIST ID*), (b) Upper and lower uncertainty limits (thick blue line) for R85, with inset illustrating temperature-dependent uncertainty factors: $f_{original}$ (blue dots) and $f_{extreme}$ (red dots), and f_{prior} (purple line).

study represents all the data better than the others, particularly in the high-temperature regime. The temperature-dependent uncertainty factors determined based on the reevaluated rate coefficient for R85 are shown in Fig. 18b, while the results for other reactions are shown in SMM 4. Also seen in Fig. 18 is the necessity of rate coefficient reevaluation for determining uncertainty factors. Defined based on the reevaluated rate coefficient, the uncertainty bands, as shown in Fig. 18b, are able to enclose almost all reported experimental and theoretical values. However, the rate coefficients from Tao et al. [14] and C3MechV3.3 [39] fall outside the physical uncertainty bands at high temperatures. If uncertainty bands are determined based on the rate coefficients from Tao et al. [14] and C3MechV3.3 [39], the uncertainty bands will certainly shift away from the uncertainty domain, undermining the fidelity of subsequent model optimization. This process is repeated for all 79 reactions, with the results for other reactions summarized in SMM 4.

The temperature-dependent uncertainty factors for each reaction can be obtained by calculating the covariance matrix of the Arrhenius parameters. This information is also beneficial for observing the uncertainty factor f (T) of interested reaction at the specific temperature, which can facilitate future efforts on model optimization. For some reactions (e.g., R407 and R441 in Fig. 19a), the rate data are very limited, making it difficult to determine the covariance matrix elements of the Arrhenius parameters. Therefore, an uncertainty factor of 2 is defined over the entire temperature range studied. Fig. 19 shows the f (T) calculated from the covariance matrix of the Arrhenius parameters for the 15 most sensitive reactions, which are averaged from the sensitivity analysis of kinetic parameters based on the IDT at T = [600, 900, 1500] K, P = 80 bar, Φ = 1. It is obvious from Fig. 19 that most reactions demonstrate higher uncertainties at low temperatures compared to high temperatures, particularly for R171: CH_3OH+O_2═CH_3O+HO_2 and R401: $CH_3CHO+HO_2$═$CH_3CO+H_2O_2$. The differences in uncertainty factors between different reactions are also significant. For instance, the uncertainty factor f (T) of R171 changes between 5.5 and 1.0 in the range of temperature 300 - 800 K, while that for R401 changes between 3.0 and 1.0 in the range of temperature 300 - 550 K. The relatively large uncertainty ranges within the low-to intermediate temperature regimes offer great potential to address the discrepancies as observed in Fig. 6.

Figs. 20a summarizes the overall deviation of the reevaluated rate coefficients from the original rate coefficients at different temperatures. The 79 reactions are evaluated at each temperature using the original

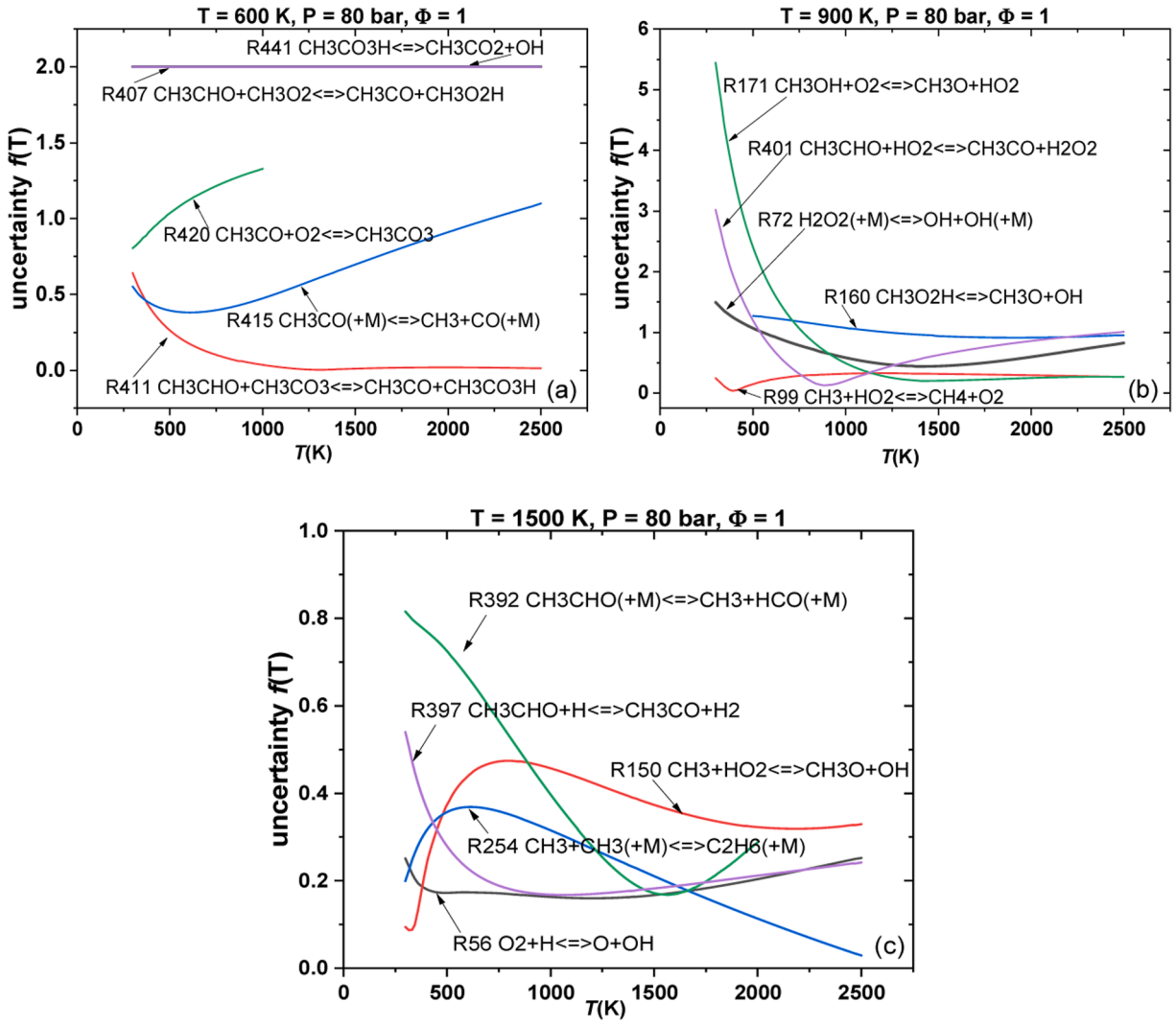

Fig. 19. Uncertainty *f*(T) curves for the investigated reactions. These lines were calculated from the covariance matrix of the Arrhenius parameters.

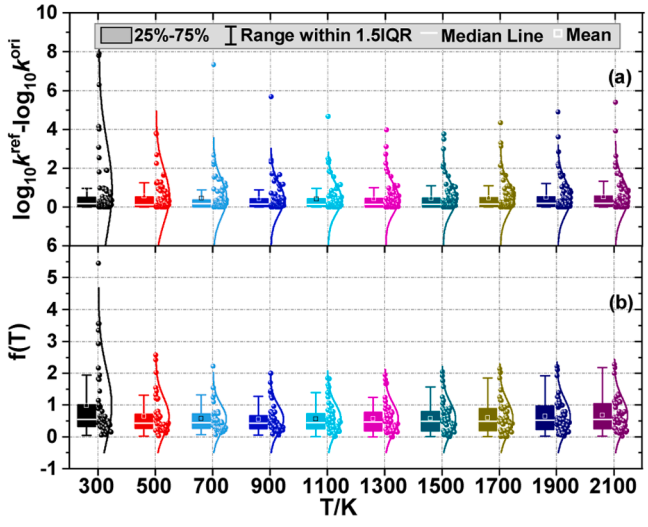

Fig. 20. Absolute values and normal distribution of (a) $\log_{10}k^{new}$-$\log_{10}k^{ori}$ and (b) the uncertainty factors *f*(T) for the 79 reactions at different temperatures.

and reevaluated rate parameters, from which the difference is computed and statistically treated with normal distribution. It can be seen from Fig. 20a that the reevaluated rate coefficient can differ from the original rate coefficient by 8 magnitude orders (i.e., at 300 K). Overall, greater differences are seen at temperatures below 1100 K (i.e., the low- and intermediate-temperature regimes). The large differences between the reevaluated and original rate coefficients, again, highlight the necessity of reevaluation based on experimental and theoretical calculation on rate parameters. Fig. 20b shows the overall distribution of rate parameter uncertainties at different temperatures, which is computed from the uncertainty factors of the 79 reactions at each temperature. Again, it is obvious from Fig. 20b that the uncertainty space for model optimization is large and that there is a high potential for the model to be optimized, particularly within the low- to intermediate-temperature regimes.

Following the above, the temperature-independent uncertainty of the thermodynamic parameters is also investigated, which represents 2σ deviations from the reevaluated values. Fig. 21 shows the uncertainty of thermochemical properties of 24 key species where the computed values are minus by the respective mean value. Several species (e.g., CH_3O, CH_3O_2, CH_3CO, CH_2CO, CH_3CO_3) clearly show greater uncertainties than their peers. Again, it is obvious from Fig. 21 that there is a large potential for the thermodynamic parameters to be optimized.

The application of the determined uncertainty domains of the key kinetic and thermodynamic parameters is further demonstrated through a case study, where the uncertainty domains are used for sampling to

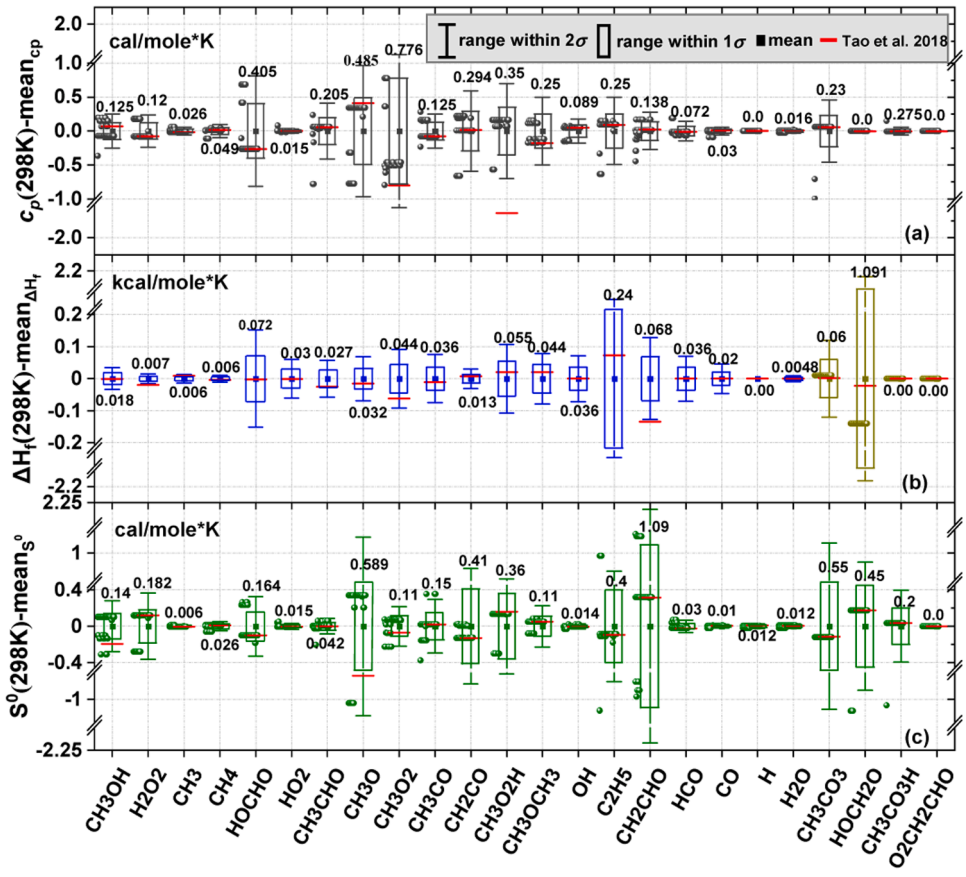

Fig. 21. Statistical distribution and uncertainty of thermochemical properties for the 24 species computed from databases and (or) 35 published chemistry models: (a) c_p(298 K), (b) Δh_f(298 K), and (c) s^0(298 K). The numbers on each column represent the absolute value of 1σ.

determine a surrogate model that maps the variables (e.g., the kinetic and thermodynamic parameters for the 79 reactions and 24 species) to the modeling targets (e.g., the experimental measurements). The uncertainty domain is further expanded in its dimension by including reactor conditions as additional parameters. Specifically, the diluent ratio, temperature, pressure and equivalence ratio are added to the kinetic and thermodynamic parameters, and are varied by [90 % - 97.5 %], [1200, 2000] K, [1, 400] bar and [0.5, 2.5], respectively, to represent the typical operation range for autoignition measurement conditions. Coupling the uncertainty domain of the reactor condition parameters with those of the kinetic and thermodynamic parameters enables the training of a single, universal surrogate model for one type of experiments (e.g., IDT measured in shock tubes). This surrogate model can be used to achieve real-time optimization of chemistry models whenever new experimental measurements from the specific reactor for the specific fuel are available. This is not achievable with most existing frameworks for model optimization, which require the training of multiple surrogate models for individual datasets. More details of such undertaking will be demonstrated in a forthcoming study from the authors' group. Thereafter, 200,000 samples are collected using Latin Hypercube Sampling [59], with each sample corresponding to a physically feasible acetaldehyde model within the model uncertainty domain (as previously determined according to Figs. 20 and 21) coupled with a fixed thermodynamic and fuel loading condition (i.e., the reactor condition). Autoignition modeling is then conducted at the 200,000 samples, from which the simulated ignition delay times are determined (defined in the same way as that used in sensitivity analysis). The 200,000 samples and the respective simulated autoignition delay times are further used to train a surrogate model using the Residual Neural Network [61] framework, similar to that adopted in [62]. An R^2 of 0.994 and mean absolute error of 0.735 are achieved over the training and test datasets, highlighting the high accuracy of the trained surrogate model.

To assess whether the surrogate model accurately captures the uncertainty of the model in predicting ignition delay times measured in shock tubes and whether the coupling between the reactor and model parameters causes any complications (e.g., overfitting or underfitting at certain reactor conditions), the surrogate model is further used quantify the uncertainty domain of the model in predicting the ignition delay time for a 0.5 % CH_3CHO/ 2.5 % O_2/ 97 % Ar mixture at $P = 3.45$ atm, $\Phi = 0.5$, and temperatures from 1200 to 2000 K. This target is selected based on the published shock tube measurements that have already been shown in Fig. 3a. 5000 samples are collected where the model parameters are randomly sampled within their respective uncertainties while the reactor condition parameters are fixed. This process is repeated from 1200 to 2000 K with a temperature interval of 100 K. These samples are then fed to the surrogate model to predict the simulated ignition delay times. The mean value and the uncertainty (2σ) from the calculated results using the surrogate model are shown in Fig. 22, along with the Zero-RK [18] predictions using the updated model. If the mean values determined from the surrogate model with the samples overlap with those predicted using Zero-RK, then the surrogate model and the coupling between the reactor and model parameters are proved to be adequate. These are confirmed in Fig. 22, where the Zero-RK predictions using the updated model (the green line) nearly coincide with the mean values determined from the surrogate model (red line).

5. Conclusion

This study aims to define a new chemical kinetic model of acetaldehyde and configure its underlying uncertainties based physical information that can be used for further model optimization. To this end, 79 elementary reactions and 24 species are identified via sensitivity

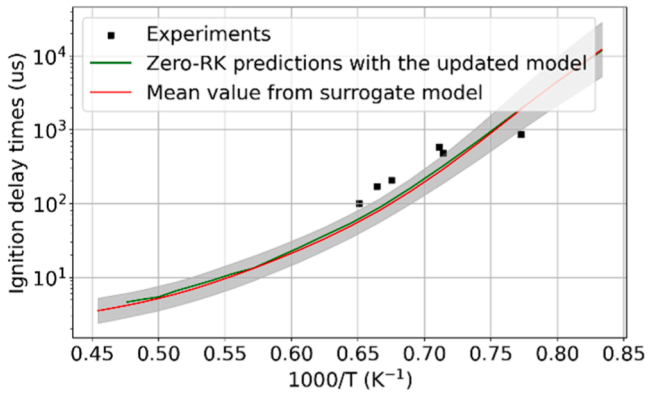

Fig. 22. Modeling uncertainty in predicted ignition delay times for a 0.5 % CH_3CHO/ 2.5 % O_2/ 97 % Ar mixture at $P = 3.45$ atm, $\Phi = 0.5$, and temperatures from 1200 to 2000 K in a shock tube. The shaded area represents the 2σ of the predictions from surrogate model at the 5000 samples, the red line represents the mean value of the surrogate model predictions, the green line represents the predictions using the updated acetaldehyde chemistry model in Zero-RK, and the symbols are the experimental data from [11].

analyses over the temperature, pressure and fuel-loading conditions that are of interest to the combustion community. The rate parameters of the 79 reactions are reevaluated using over 100,000 direct experiments and quantum chemistry computations from > 900 studies, and the thermochemistry (Δh_f(298 K), s^0(298 K) and c_p) are reevaluated based on the ATCT database, the NIST Chemistry WebBook, the TMTD database, and 35 published chemistry models.

The updated rate parameters and thermochemistry are incorporated into a recent acetaldehyde chemistry model, which is further assessed against available fundamental experiments, including 10 ignition delay times in RCM, 123 ignition delay times in shock tube, 633 species concentrations in JSR, and 102 species concentrations in flow reactor. Five published acetaldehyde models are also adopted for comparison. Surprisingly, the updated model, though not calibrated against the fundamental experiments, are equal to or better than the previous models, despite the large differences in kinetic and thermochemical parameters of the key reactions and species, respectively. The new model clearly better reproduces the experiments in the high-temperature regime, with significant discrepancies observed within the low- to intermediate-temperature regimes that require further attention. Sensitivity and flux analyses are further performed, with considerably changed branching ratios in the updated model observed for the consuming pathways of CH_3CHO and CH_2O. There is a clear shift toward H-atom abstractions by OH radicals for CH_3CHO and CH_2O consumption, with greatly promoted CH_2CHO formation.

The large differences between the updated rate coefficients and the original values adopted in the existing chemistry models reveal the necessity of reassessment of key reactions in the core chemistry completely based on direct experiments and theoretical calculations for rate parameters. Following this, based on these datasets, as well as recommended values from review articles, the temperature-dependent and temperature-independent uncertainties are statistically evaluated for kinetic and thermochemical parameters, respectively. The application of the determined uncertainty domains of the key kinetic and thermodynamic parameters is further demonstrated through a case study, where the surrogate model accurately captures the uncertainty of the updated model in predicting ignition delay times in a shock tube.

Since the model uncertainty is representative of the uncertainties of the rate and thermodynamic parameters and the nominal model can be considered as a statistical representation of its uncertainty, a unified framework for real-time UQ and optimization can be developed with minimized probability of data inconsistency, which will be demonstrated in a forthcoming study from the author's group where the observed discrepancies between the updated model and the fundamental experiments (particularly those in the low- to intermediate-temperature regimes) will be minimized.

CRediT authorship contribution statement

Xinrui Ren: Writing – original draft, Software, Methodology, Investigation, Conceptualization. **Hongqing Wu:** Methodology, Investigation. **Ruoyue Tang:** Methodology, Investigation. **Yanqing Cui:** Methodology, Investigation. **Mingrui Wang:** Methodology, Investigation. **Song Cheng:** Writing – review & editing, Methodology, Investigation, Funding acquisition, Conceptualization.

Declaration of competing interest

The authors declare that they have no known competing financial interests or personal relationships that could have appeared to influence the work reported in this paper.

Acknowledgments

The work described in this paper was supported by grants from the Research Grants Council of the Hong Kong Special Administrative Region, China (PolyU P0046985 for ECS project funded in 2023/24 Exercise and P0050998), and by the Natural Science Foundation of Guangdong Province under 2023A1515010976.

Supplementary materials

Supplementary material associated with this article can be found, in the online version, at doi:10.1016/j.jaecs.2025.100320.

Data availability

Data will be made available on request.

References

[1] Tang R, Han Y, Chen H, Qu B, Li Y, Lu Z, Xing Z, Cheng S. Theoretical study of H-atom abstraction by CH3OȮ radicals from aldehydes and alcohols: *ab initio* and comprehensive kinetic modeling. Combust Flame 2024;259:113175. https://doi.org/10.1016/j.combustflame.2023.113175.
[2] Cheng S, Kang D, Goldsborough SS, Saggese C, Wagnon SW, Pitz WJ. Experimental and modeling study of C2–C4 alcohol autoignition at intermediate temperature conditions. Proc Combust Inst 2021;38:709–17. https://doi.org/10.1016/j.proci.2020.08.005.
[3] Sarathy SM, Oßwald P, Hansen N, Kohse-Höinghaus K. Alcohol combustion chemistry. Prog Energy Combust Sci 2014;44:40–102. https://doi.org/10.1016/j.pecs.2014.04.003.
[4] Rice FO, Herzfeld KF. The thermal decomposition of organic compounds from the standpoint of free radicals. VI. The mechanism of some chain reactions. J Am Chem Soc 1934;56:284–9. https://doi.org/10.1021/ja01317a006.
[5] Beeley P, Griffiths JF, Hunt BA, Williams A. The combustion of acetaldehyde behind incident shock waves. Symp Int Combust 1977;16:1013–22. https://doi.org/10.1016/S0082-0784(77)80392-5.
[6] Kaiser EW, Westbrook CK, Pitz WJ. Acetaldehyde oxidation in the negative temperature coefficient regime: experimental and modeling results. Int J Chem Kinet 1986;18:655–88. https://doi.org/10.1002/kin.550180606.
[7] Borisov BD, Gribanov IV. Recording of spectral line shapes in time. J Appl Spectrosc 1990;53:748–51. https://doi.org/10.1007/BF00665147.
[8] Dagaut P, Reuillon M, Voisin D, Cathonnet M, Mcguinness M, Simmie JM. Acetaldehyde oxidation in a JSR and ignition in shock waves: experimental and comprehensive kinetic modeling. Combust Sci Technol 1995;107:301–16. https://doi.org/10.1080/00102209508907809.
[9] Won SJ, Ryu JC, Bae JH, Kim YD, Gang JG. Shock-tube study of the oxidation of acetaldehyde at high temperature. Bull Korean Chem Soc 2000;21:487–92. https://doi.org/10.5012/bkcs.2000.21.5.487.
[10] Yasunaga K, Kubo S, Hoshikawa H, Kamesawa T, Hidaka Y. Shock-tube and modeling study of acetaldehyde pyrolysis and oxidation. Int J Chem Kinet 2008;40:73–102. https://doi.org/10.1002/kin.20294.
[11] Mével R, Chatelain K, Blanquart G, Shepherd JE. An updated reaction model for the high-temperature pyrolysis and oxidation of acetaldehyde. Fuel 2018;217:226–39. https://doi.org/10.1016/j.fuel.2017.12.060.
[12] Tao T, Sun W, Yang B, Hansen N, Moshammer K, Law CK. Investigation of the chemical structures of laminar premixed flames fueled by acetaldehyde. Proc Combust Inst 2017;36:1287–94. https://doi.org/10.1016/j.proci.2016.05.030.

[13] Zhang X, Ye L, Li Y, Zhang Y, Cao C, Yang J, Zhou Z, Huang Z, Qi F. Acetaldehyde oxidation at low and intermediate temperatures: an experimental and kinetic modeling investigation. Combust Flame 2018;191:431–41. https://doi.org/10.1016/j.combustflame.2018.01.027.

[14] Tao T, Kang S, Sun W, Wang J, Liao H, Moshammer K, Hansen N, Law CK, Yang B. A further experimental and modeling study of acetaldehyde combustion kinetics. Combust Flame 2018;196:337–50. https://doi.org/10.1016/j.combustflame.2018.06.007.

[15] Tao T, Sun W, Hansen N, Jasper AW, Moshammer K, Chen B, Wang Z, Huang C, Dagaut P, Yang B. Exploring the negative temperature coefficient behavior of acetaldehyde based on detailed intermediate measurements in a jet-stirred reactor. Combust Flame 2018;192:120–9. https://doi.org/10.1016/j.combustflame.2018.01.048.

[16] Hashemi H, Christensen JM, Marshall P, Glarborg P. Acetaldehyde oxidation at elevated pressure. Proc Combust Inst 2021;38:269–78. https://doi.org/10.1016/j.proci.2020.06.311.

[17] Wako FM, Pio G, Salzano E. Modelling of acetaldehyde and acetic acid combustion. Combust Theory Model 2023;27:536–57. https://doi.org/10.1080/13647830.2023.2178973.

[18] Cheng S, Saggese C, Kang D, Goldsborough SS, Wagnon SW, Kukkadapu G, Zhang K, Mehl M, Pitz WJ. Autoignition and preliminary heat release of gasoline surrogates and their blends with ethanol at engine-relevant conditions: experiments and comprehensive kinetic modeling. Combust Flame 2021;228:57–77. https://doi.org/10.1016/j.combustflame.2021.01.033.

[19] Frenklach M, Packard A, Seiler P, Feeley R. Collaborative data processing in developing predictive models of complex reaction systems. Int J Chem Kinet 2004;36:57–66. https://doi.org/10.1002/kin.10172.

[20] Sheen DA, Wang H. The method of uncertainty quantification and minimization using polynomial chaos expansions. Combust Flame 2011;158:2358–74. https://doi.org/10.1016/j.combustflame.2011.05.010.

[21] Turányi T, Nagy T, Zsély IGy, Cserháti M, Varga T, Szabó BT, Sedyó I, Kiss PT, Zempléni A, Curran HJ. Determination of rate parameters based on both direct and indirect measurements. Int J Chem Kinet 2012;44:284–302. https://doi.org/10.1002/kin.20717.

[22] Wang J, Zhou Z, Lin K, Law CK, Yang B. Facilitating Bayesian analysis of combustion kinetic models with artificial neural network. Combust Flame 2020;213:87–97. https://doi.org/10.1016/j.combustflame.2019.11.035.

[23] Slavinskaya NA, Abbasi M, Starcke JH, Whitside R, Mirzayeva A, Riedel U, Li W, Oreluk J, Hegde A, Packard A, Frenklach M, Gerasimov G, Shatalov O. Development of an uncertainty quantification predictive chemical reaction model for syngas combustion. Energy Fuels 2017;31:2274–97. https://doi.org/10.1021/acs.energyfuels.6b02319.

[24] H. Wang, X. You, A.V. Joshi, S.G. Davis, A. Laskin, F. Egolfopoulos, C.K. Law, U.M. Version II, high-temperature combustion reaction model of H2/CO/C1–C4 compounds, (2007).

[25] Olm C, Varga T, Valkó É, Curran HJ, Turányi T. Uncertainty quantification of a newly optimized methanol and formaldehyde combustion mechanism. Combust Flame 2017;186:45–64. https://doi.org/10.1016/j.combustflame.2017.07.029.

[26] Ren X, Bai X, Jia M, Liu S, Han Y, Tang R, Cheng S, Zhou C-W, Curran HJ, Li Y. *Ab initio* kinetics for H-atom abstraction from C1–C5 hydrocarbon and oxygenated species by CH3Ȯ radicals. Combust Flame 2024;263:113410. https://doi.org/10.1016/j.combustflame.2024.113410.

[27] Turányi T. Sensitivity analysis of complex kinetic systems. Tools and applications. J Math Chem 1990;5:203–48. https://doi.org/10.1007/BF01166355.

[28] vom Lehn F, Cai L, Pitsch H. Sensitivity analysis, uncertainty quantification, and optimization for thermochemical properties in chemical kinetic combustion models. Proc Combust Inst 2019;37:771–9. https://doi.org/10.1016/j.proci.2018.06.188.

[29] NIST Chemical Kinetics Database, 2025. https://kinetics.nist.gov/kinetics/. (accessed March 22, 2024).

[30] Olm C, Varga T, Valkó É, Hartl S, Hasse C, Turányi T. Development of an ethanol combustion mechanism based on a hierarchical optimization approach. Int J Chem Kinet 2016;48:423–41. https://doi.org/10.1002/kin.20998.

[31] Konnov AA. Remaining uncertainties in the kinetic mechanism of hydrogen combustion. Combust Flame 2008;152:507–28. https://doi.org/10.1016/j.combustflame.2007.10.024.

[32] Baulch DL, Bowman CT, Cobos CJ, Cox RA, Just Th, Kerr JA, Pilling MJ, Stocker D, Troe J, Tsang W, Walker RW, Warnatz J. Evaluated kinetic data for combustion modeling: supplement II. J Phys Chem Ref Data 2005;34:757–1397. https://doi.org/10.1063/1.1748524.

[33] Hong Z, Davidson DF, Hanson RK. An improved H2/O2 mechanism based on recent shock tube/laser absorption measurements. Combust Flame 2011;158:633–44. https://doi.org/10.1016/j.combustflame.2010.10.002.

[34] Kéromnès A, Metcalfe WK, Heufer KA, Donohoe N, Das AK, Sung C-J, Herzler J, Naumann C, Griebel P, Mathieu O, Krejci MC, Petersen EL, Pitz WJ, Curran HJ. An experimental and detailed chemical kinetic modeling study of hydrogen and syngas mixture oxidation at elevated pressures. Combust Flame 2013;160:995–1011. https://doi.org/10.1016/j.combustflame.2013.01.001.

[35] Burke MP, Chaos M, Ju Y, Dryer FL, Klippenstein SJ. Comprehensive H2/O2 kinetic model for high-pressure combustion. Int J Chem Kinet 2012;44:444–74. https://doi.org/10.1002/kin.20603.

[36] Ruscic B, Pinzon RE, von Laszewski G, Kodeboyina D, Burcat A, Leahy D, Montoy D, Wagner AF. Active thermochemical tables: thermochemistry for the 21st century. J Phys Conf Ser 2005;16:561. https://doi.org/10.1088/1742-6596/16/1/078.

[37] Burcat A, Ruscic B. Third millenium ideal gas and condensed phase thermochemical database for combustion (with update from active thermochemical tables). Argonne, IL (United States): Argonne National Lab. (ANL); 2005. https://doi.org/10.2172/925269.

[38] Kovács M, Papp M, Zsély IGy, Turányi T. Main sources of uncertainty in recent methanol/NOx combustion models. Int J Chem Kinet 2021;53:884–900. https://doi.org/10.1002/kin.21490.

[39] Dong S, Wagnon SW, Pratali Maffei L, Kukkadapu G, Nobili A, Mao Q, Pelucchi M, Cai L, Zhang K, Raju M, Chatterjee T, Pitz WJ, Faravelli T, Pitsch H, Senecal PK, Curran HJ. A new detailed kinetic model for surrogate fuels: C3MechV3.3. Appl Energy Combust Sci 2022;9:100043. https://doi.org/10.1016/j.jaecs.2021.100043.

[40] Keyser LF. Kinetics of the reaction OH+HO2->H2O+O2 from 254 to 382 K. J Phys Chem 1988;92:1193–200. https://doi.org/10.1021/j100316a037.

[41] Peeters J, Mahnen G. Reaction mechanisms and rate constants of elementary steps in methane-oxygen flames. Symp Int Combust 1973;14:133–46. https://doi.org/10.1016/S0082-0784(73)80015-3.

[42] Zhao Z, Wang Y, Zhang J, Liang J, Zhang Y, Zhao F, Wang Q-D. A shock-tube experimental and kinetic simulation study on the autoignition of methane at ultra-lean and lean conditions. Heliyon 2024;10:e34204. https://doi.org/10.1016/j.heliyon.2024.e34204.

[43] Hu E, Pan L, Gao Z, Lu X, Meng X, Huang Z. Shock tube study on ignition delay of hydrogen and evaluation of various kinetic models. Int J Hydrog Energy 2016;41:13261–80. https://doi.org/10.1016/j.ijhydene.2016.05.118.

[44] Hong Z, Davidson DF, Lam K-Y, Hanson RK. A shock tube study of the rate constants of HO2 and CH3 reactions. Combust Flame 2012;159:3007–13. https://doi.org/10.1016/j.combustflame.2012.04.009.

[45] Ryu S-O, Shin KS, Hwang SM. Determination of the rate coefficients of the CH + O → HO + CH and HCO + O → HO + CO reactions at high temperatures. Bull Korean Chem Soc 2017;38:228–36. https://doi.org/10.1002/bkcs.11070.

[46] Shaw R. Semi-empirical extrapolation and estimation of rate constants for abstraction of H from methane by H, O, HO, and O2. J Phys Chem Ref Data 1978;7:1179–90. https://doi.org/10.1063/1.555577.

[47] Skinner GB, Lifshitz A, Scheller K, Burcat A. Kinetics of methane oxidation. J Chem Phys 1972;56:3853–61. https://doi.org/10.1063/1.1677790.

[48] Keiffer M, Miscampbell AJ, Pilling MJ. A global technique for analysing multiple decay curves. Application to the CH3+ O2 system. J Chem Soc Faraday Trans 2 Mol Chem Phys 1988;84:505–14. https://doi.org/10.1039/F29888400505.

[49] Parkes DA. The oxidation of methyl radicals at room temperature. Int J Chem Kinet 1977;9:451–69. https://doi.org/10.1002/kin.550090313.

[50] Pilling MJ, Smith MJC. A laser flash photolysis study of the reaction methyl + molecular oxygen .fwdarw. Methylperoxy (CH3O2) at 298 K. J Phys Chem 1985;89:4713–20. https://doi.org/10.1021/j100268a014.

[51] Castañeda R, Iuga C, Álvarez-Idaboy JR, Vivier-Bunge A. Rate constants and branching ratios in the oxidation of aliphatic aldehydes by OH radicals under atmospheric conditions. J Mex Chem Soc 2012;56:316–24. http://www.scielo.org.mx/scielo.php?script=sci_abstract&pid=S1870-249X2012000300014&lng=es&nrm=iso&tlng=en (accessed December 5, 2024).

[52] Tyndall GS, Staffelbach TA, Orlando JJ, Calvert JG. Rate coefficients for the reactions of OH radicals with methylglyoxal and acetaldehyde. Int J Chem Kinet 1995;27:1009–20. https://doi.org/10.1002/kin.550271006.

[53] Cox RA, Derwent RG, Holt PM, Kerr JA. Photolysis of nitrous acid in the presence of acetaldehyde. J Chem Soc Faraday Trans 1 Phys Chem Condens Phases 1976;72:2061–75. https://doi.org/10.1039/F19767202061.

[54] Altarawneh M, Al-Muhtaseb AH, Dlugogorski BZ, Kennedy EM, Mackie JC. Rate constants for hydrogen abstraction reactions by the hydroperoxyl radical from methanol, ethenol, acetaldehyde, toluene, and phenol. J Comput Chem 2011;32:1725–33. https://doi.org/10.1002/jcc.21756.

[55] Colket MB, Naegeli DW, Glassman I. High temperature oxidation of acetaldehyde. Symp Int Combust 1977;16:1023–39. https://doi.org/10.1016/S0082-0784(77)80393-7.

[56] Mousavipour SH, Saheb V. Theoretical study on the kinetic and mechanism of H+HO2 reaction. Bull Chem Soc Jpn 2007;80:1901–13. https://doi.org/10.1246/bcsj.80.1901.

[57] Bates RW, Golden DM, Hanson RK, Bowman CT. Experimental study and modeling of the reaction H + O2+ M → HO2+ M (M = Ar, N2, H2O) at elevated pressures and temperatures between 1050 and 1250 K. Phys Chem Chem Phys 2001;3:2337–42. https://doi.org/10.1039/B010002L.

[58] Michael JV, Su M-C, Sutherland JW, Carroll JJ, Wagner AF. Rate constants for H + O2 + M → HO2 + M in seven bath gases. J Phys Chem A 2002;106:5297–313. https://doi.org/10.1021/jp020229w.

[59] Cheng S, Yang Y, Brear MJ, Frenklach M. Quantifying uncertainty in kinetic simulation of engine autoignition. Combust Flame 2020;216:174–84. https://doi.org/10.1016/j.combustflame.2020.02.025.

[60] Nagy T, Valkó É, Sedyó I, Zsély IGy, Pilling MJ, Turányi T. Uncertainty of the rate parameters of several important elementary reactions of the H2 and syngas combustion systems. Combust Flame 2015;162:2059–76. https://doi.org/10.1016/j.combustflame.2015.01.005.

[61] K. He, X. Zhang, S. Ren, J. Sun, Deep residual learning for image recognition, in: 2016: pp. 770–8. https://openaccess.thecvf.com/content_cvpr_2016/html/He_Deep_Residual_Learning_CVPR_2016_paper.html (accessed May 27, 2024).

[62] Zhang Y, Dong W, Vandewalle LA, Xu R, Smith GP, Wang H. Neural network approach to response surface development for reaction model optimization and uncertainty minimization. Combust Flame 2023;251:112679. https://doi.org/10.1016/j.combustflame.2023.112679.